

THESIS FOR THE DEGREE OF DOCTORATE OF ENGINEERING

**CARBON NANOTUBE BASED INTERCONNECT MATERIALS
FOR ELECTRONIC APPLICATIONS**

DI JIANG



CHALMERS

Department of Microtechnology and Nanoscience
Chalmers University of Technology
Gothenburg, Sweden
2015

Carbon Nanotube Based Interconnect Materials for Electronic Applications

Di Jiang

ISBN: 978-91-7597-305-0

©Di Jiang, 2015

Doktorsavhandlingar vid Chalmers tekniska högskola

Ny serie nr 3986

ISSN 0346-718X.

EMSL

Department of Microtechnology and Nanoscience (MC2)

Chalmers University of Technology

SE-412 96 Gothenburg, Sweden

Telephone +46 (0) 31 772 1000

ISSN 1652-0769

Technical Report MC2-329

ABSTRACT

Carbon nanotubes (CNTs) are considered as a candidate material for future electronic interconnect applications. This thesis summarizes the research work on the fabrication and characterization of CNT-based interconnect systems, and explores the possibilities of integrating CNTs into various electronic interconnect scenarios.

CNT material properties and fabrication methods are introduced as well as its potential for solving the future interconnect challenges. The technology development works are presented in detail in four categories: synthesis, densification, coating and transfer.

The principles of the chemical vapor deposition (CVD) method for producing the CNTs are described and discussed. Densification methods are developed in order to increase the volume density of the pristine porous CVD-grown CNTs. Two techniques, vapor-based densification and paper-mediated wet densification, have been proposed and characterized. CNT transfer techniques are developed in order to decouple the harsh CVD growth environment from the target application devices. Two kinds of transfer medium materials, indium and polymer, have been proposed and optimized. To improve the electrical performance of the pristine CNTs, metallic coating techniques for both vertically aligned and randomly dispersed CNTs are developed and characterized.

Finally, three different CNT-based interconnect scenarios: bumps, through silicon vias, and flexible conductors, are demonstrated and characterized, using the as-developed processes. The integration technologies developed in this thesis not only improve the CNT process compatibility with the conventional electronics manufacture flows, but also offers state-of-the-art electrical and mechanical performance for the non-conventional flexible and stretchable interconnect applications.

Keywords: carbon nanotube; electronics packaging; electrical interconnect; bump; through silicon via; three dimensional integration; densification; transfer; flexible electronics

To my family, especially to Xin

LIST OF PUBLICATIONS

Paper A

Formation of Three-dimensional Carbon Nanotube Structures by Controllable Vapor Densification

Teng Wang, Di Jiang, Si Chen, Kjell Jeppson, Lilei Ye, Johan Liu
Materials Letters, Volume 78, Pages 184-187, 2012

Paper B

Through-Silicon Vias Filled With Densified and Transferred Carbon Nanotube Forests

Teng Wang, Si Chen, Di Jiang, Yifeng Fu, Kjell Jeppson, Lilei Ye, Johan Liu
IEEE Electron Device Letters, Volume 33, Issue 3, Pages 420-422, 2012

Paper C

Paper-mediated Controlled Densification and Low Temperature Transfer of Carbon Nanotube Forests for Electronic Interconnect Application

Di Jiang, Teng Wang, Si Chen, Lilei Ye, Johan Liu
Microelectronic Engineering, Volume 103, Pages 177-180, 2013

Paper D

Vertically Stacked Carbon Nanotube-Based Interconnects for Through Silicon Via Application

Di Jiang, Wei Mu, Si Chen, Yifeng Fu, Kjell Jeppson, Johan Liu
IEEE Electron Device Letters, Volume 36, Issue 5, Pages 499-501, 2015

Paper E

Flexible Multifunctionalized Carbon Nanotubes-Based Hybrid Nanowires

Nan Wang, Di Jiang, Lilei Ye, Murali Murugesan, Michael Edwards, Yifeng Fu, Johan Liu
Advanced Functional Materials, Volume 25, Issue 26, Pages 4135-4143, 2015

Paper F

Embedded Fin-like Metal/CNT Hybrid Structures for Flexible and Transparent Conductors

Di Jiang, Nan Wang, Michael Edwards, Wei Mu, Andreas Nylander, Yifeng Fu, Kjell Jeppson, Johan Liu
Accepted by Small.

Paper G

Flexible 3D Stackable Interconnect System using Growth-Engineered Carbon Nanotube Scaffold

Di Jiang, Nan Wang, Shuangxi Sun, Kjell Jeppson, Michael Edwards, Yifeng Fu, Johan Liu

In manuscript. Submitted for publication.

Other contributions that are not included in the discussion due to being out of the scope of this thesis:

- **Carbon Nanotubes in Electronics Interconnect Applications with a Focus on 3D-TSV Technology**

Di Jiang, Teng Wang, Lilei Ye, Kjell Jeppson, Johan Liu, ECS Transactions, Volume 44, Issue 1, Pages 683-692, 2012

- **Experimental and Numerical Investigations on the Performance and Reliability of CNT Fins for Micro-cooler**

Yan Zhang, Huifeng Lv, Jingyu Fan, Di Jiang, Johan Liu, Proceedings of the IEEE CPMT International Conference on Electronic Packaging Technology & High Density Packaging, Pages 1573-1577, 2012

- **Room Temperature Transfer of Carbon Nanotubes on Flexible Substrate**

Di Jiang, Yifeng Fu, Yan Zhang, Johan Liu, Proceedings of the 18th Thermionic International Workshop on Thermal Investigations of ICs and Systems, Pages 213-216, 2012

- **Controlling the Density of CNTs by Different Underlayer Materials in PECVD Growth**

Liang Xu, Di Jiang, Yifeng Fu, Shantung Tu, Johan Liu, Proceedings of the 19th International Workshop on Thermal Investigations of ICs and Systems (THERMINIC), Pages 248-252, 2013

CONTENTS

1	INTRODUCTION	1
1.1	Background	1
1.2	Outline	2
2	CARBON NANOTUBE BASICS	3
2.1	Electrical Properties	3
2.2	Thermal Properties	4
2.3	Mechanical Properties	5
2.4	Carbon Nanotube Synthesis	5
3	TECHNOLOGY DEVELOPMENT	7
3.1	Chemical Vapor Deposition of Carbon Nanotubes	7
3.2	Densification of Carbon Nanotubes	11
3.3	Transfer of Carbon Nanotubes	18
3.4	Metallic Coating of Carbon Nanotubes	22
4	APPLICATIONS	29
4.1	Bump Interconnects	29
4.2	Through Silicon Vias	30
4.3	Flexible and Stretchable Interconnects	32
4.4	Flexible and Transparent Interconnects	34
4.5	3D Interconnects for Flexible Circuit Integration	37
5	CONCLUSION	41
	Acknowledgment	43
	BIBLIOGRAPHY	45

ACRONYMS

CNT Carbon nanotubes

TSV through silicon via

PCB printed circuit board

LED light emitting diodes

TEM transmission electron microscopy

SEM scanning electron microscope

CVD chemical vapor deposition

DRIE deep reactive ion etching

CTE coefficient of thermal expansion

BCB benzocyclobutene

PDMS polydimethylsiloxane

PMMA polymethyl methacrylate

INTRODUCTION

1.1 BACKGROUND

Interconnect, which servers the purpose of exchanging signals between various components, is one of the most critical parts of an electronic system. In most electronic systems, metals are the dominant materials for making the interconnect. For example, copper and aluminum are extensively used as the microelectronics interconnect. Copper traces with nickel and gold finish are commonly used on a printed circuit board (PCB). And copper cores can be found in almost all the electrical cables.

As the metal interconnect technology gets mature, it is reaching its physical limitations in many applications. For example, at nanometer scales, copper interconnect becomes more resistive and suffers performance decrease due to grain boundaries scattering, line edge roughness and undesirable diffusion [1]. Copper through silicon via (TSV) suffers from its mismatch of coefficient of thermal expansion (CTE) with silicon substrates [2]. Furthermore, in many emerging applications, like the flexible, transparent and stretchable electronics [3], metals have very limited fatigue resistance and stretchability [4] which are critical in the success of these new devices.

Carbon nanotubes (CNT), which were brought into the research spotlight in the 1990s [5], are considered as one of the promising materials to build future electronic interconnect systems. CNTs are mechanically flexible and resilient, and have very low thermal expansion. The maximum current carrying capacity of the CNTs can be up to 10^9 A/cm² [6–8], much higher than that of copper. CNTs are reliable because they have high resistance to electromigration and have very low Joule heating. Moreover, they are thermally conductive and stable. These advantages have already triggered intensive research on developing CNT-based interconnects [9–18]. However, despite of the numerous efforts spent, this new material has not yet been transitioned from academia to industry, mainly due to CNT's incompatible synthesis conditions, imperfect synthesis products and difficulties in manipulating the synthesis results.

As part of the efforts to remove the obstacles hindering the exploitation of the CNT-based interconnects, this thesis focuses mostly on the process development works that shall be required for the realization of functional CNT interconnect

1.2 OUTLINE

systems. Demonstrative interconnect systems have been realized at scales from micrometers to millimeters, which are related to the potential applications at the package level and the system level.

1.2 OUTLINE

This thesis is organized into five chapters. Chapter 1 gives a general introduction to the the background and outline of this thesis. Chapter 2 provides a general introduction to the basics of the CNT materials. In chapter 3, the CNT process development works are discussed in detail, including the synthesis, densification, transfer and metallic coating of the nanotubes, with the aim to improve the quality of the CNTs and to make the fabrication processes comply with the established technologies. In chapter 4, the individual processes discussed in chapter 3 are selectively combined and application-specific CNT interconnect demonstrators, i.e. bumps, through silicon vias and flexible conductors, are fabricated and characterized. Lastly, chapter 5 provides a summary of this thesis.

2

CARBON NANOTUBE BASICS

Carbon nanotubes (CNT) can be considered as hollow long tubes composed of rolled single-atom layers of graphite (also called graphene). A single-wall CNT consists of just one layer of graphene, while a multi-wall CNT consists of two or more layers (Figure 2.1a).

A graphene layer can be rolled into tubes in different directions. This is represented by a pair of indices (n,m) which is called the chirality (Figure 2.1b). According to different n and m , CNTs can be classified into three different types: zig-zag if $m=0$, armchair if $n=m$, and chiral for the rest of the combinations. The electrical, thermal and mechanical properties of the CNT, concerning its use as an interconnect material, are discussed as follows.

2.1 ELECTRICAL PROPERTIES

A single-wall CNT can be either metallic or semiconductive depending on its chirality [20]. As shown in Figure 2.1b, A single-wall CNT with the chirality indices (n,m) satisfying $n - m = 3i$, where i is an integer, exhibits metallic behavior in conducting electrons. Single-wall CNTs with all other chiralities are semiconductive with a band gap approximately inversely proportional to the tube diameter [21–23]. Armchair single-wall CNTs ($n = m$) are always metallic. Other metallic single-wall CNTs ($n - m = 3i$, where $i \neq 0$) have a small band gap of 2 to 50 meV induced by the curvature of the tube [6]. When synthesized in large quantities, one third of the produced single-wall CNTs are statistically metallic, while two thirds are semiconductive. In the case of multi-wall CNTs, the same principle applies to the walls of one tube. Multi-wall CNTs have been experimentally shown to have multichannel conduction [24]. Opening the ends of the multi-wall CNT using etching [25, 26] and polishing [27] can make the inner shells available to electron conduction. The CNTs used in this thesis are all multi-wall CNTs.

If the length of a conductive single-wall CNT is shorter than its electron mean free path, it will behave as a quantum conductor with twice of a quantum conductance ($G_0 = 2e^2/h$, where e is the elementary charge and h is Planck's constant [6]). Therefore, in principle the minimum resistance of a single-wall CNT is $h/4e^2 = 6.45 k\Omega$. The electron mean free path of a CNT at room temperature can be up to a few tens of micrometers [28, 29].

2.2 THERMAL PROPERTIES

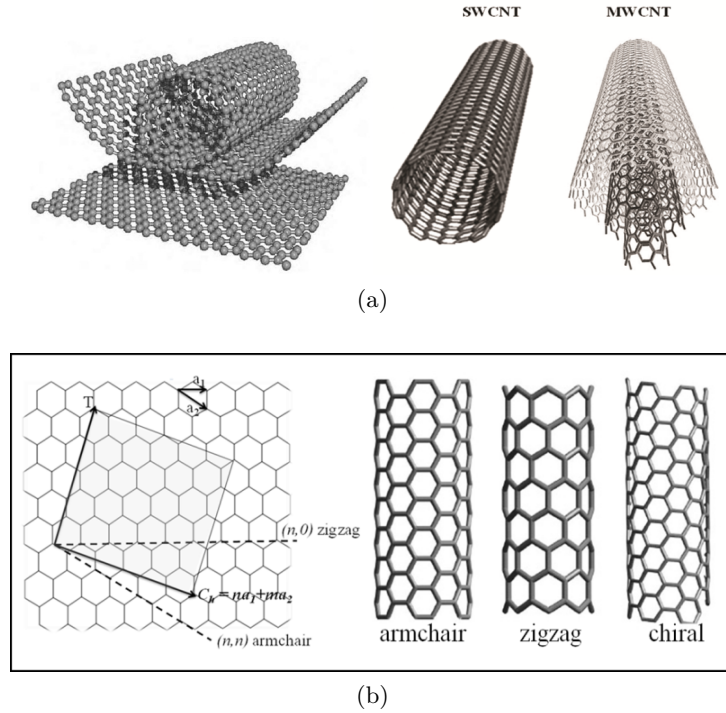


Figure 2.1: Modeling of the CNTs. (a) One CNT can be considered as the graphene sheet rolled up. (b) Different chiralities of the CNTs. (reference [19])

CNTs also have some other unique electrical properties. Individual CNTs can carry a current density up to 10^9 A/cm² [6–8], which is a few orders of magnitude higher than that of copper. CNTs have not been observed to fail due to electromigration [30]. The Joule heating in CNTs is significantly less than predicted by Joule’s law [31].

It should be noted that the CNTs with defects show much higher electrical resistance than the perfect CNTs [32], which triggers many research efforts, including this thesis, to make up for these imperfections.

2.2 THERMAL PROPERTIES

CNTs possess exceptionally high thermal conductivity of more than 3000 W/mK at room temperature [33, 34], higher than those of copper (~ 400 W/mK) and diamond (~ 2000 W/mK). These results agree well with the theoretical calculations and modeling works [35–37] on the thermal properties of CNTs. Similar to the electron transport, it should be pointed out that the defects and vacancies in the CNTs significantly decrease their thermal conductivity [36].

2.3 MECHANICAL PROPERTIES

CNT is a very strong material due to the strong covalent sp^2 bonds between the carbon atoms. The Young's modulus of the single-wall CNTs and multi-wall CNTs are both in the TPa range (3.6 TPa for single-wall CNTs and 2.4 TPa for multi-wall CNTs [38–40]). Theoretical work has predicted values in a similar range [41–43]. The tensile strength of CNT is in the range of a few tens of GPa [39, 40, 44]. The CNTs are mechanically anisotropic as their Young's modulus in the transverse direction is much lower than that in the axial direction for CNTs with large diameters [45]. CNTs have low thermal expansion close to zero [46], which matches well with that of silicon ($2.6 \times 10^{-6} \text{ K}^{-1}$), compared with copper at around $16 \times 10^{-6} \text{ K}^{-1}$ and aluminum around $22 \times 10^{-6} \text{ K}^{-1}$ at the room temperature. In the macro scale, on the other hand, CNTs are also quite flexible and resilient [47].

2.4 CARBON NANOTUBE SYNTHESIS

CNT synthesis is typically a multi-step chemical process in which carbon is deposited in solid form. This conversion occurs at the nano scale via endothermic reactions occurring at the surface of the catalyst nano-particles. The catalyst is added either in the form of nano-scale deposition on a substrate or freely floating nano-particle aerosol embedded in the bulk phase. The most common methods for making CNTs are: 1) plasma arc discharge, 2) laser ablation, and 3) chemical vapor deposition (CVD).

Sumio Iijima used the arc discharge method for the early discovery and identification of CNTs in the 1990s [5]. The process involved condensation of carbon atoms generated from evaporation of a solid carbon source. In this method, high electric currents (about 50 to 120 A) are passed through the graphite electrodes placed at a distance of approximately 1 mm in the synthesis chamber, causing the material from the cathode to sublime and the nanotubes to form on the anode. The arc discharge process has very high temperature ($\sim 3200 \text{ K}$) in the electrode gap, which usually requires a lot of energy input, and hence is expensive. Unwanted byproducts such as polyhedron graphite particles may contaminate the CNT products.

In the laser ablation method [48], a high energy laser is directed to ablate a carbon target, which contains nickel or cobalt catalyst, in a tube furnace at the temperature of around 1400 K. A flow of inert gas is passed through the chamber to carry the CNTs downstream, to a collector surface. The CNTs formed by the laser ablation method are of higher quality than those produced by the arc discharge method. However, the laser ablation method is not cheap either, because it requires a lot of energy as well.

In the CVD method, CNTs are chemically synthesized (also referred to as “grown”) by the decomposition of a hydrocarbon gas over transition metal catalysts, such as

2.4 CARBON NANOTUBE SYNTHESIS

Method name	Reaction temperature (°C)	CNT length (μm)	Growth rate (μm/sec)	CNT quality	Purity
Arc discharge	~ 4000	1	Up to 10^7	High	Low
Laser ablation	~ 1000	~ 1	~ 0.1	High	Med
CVD	500-1200	0.1 - 10^5	0.1 - 10	Med	Med-high

Table 2.1: Summary of the CNT synthesis methods. (data based on reference [49])

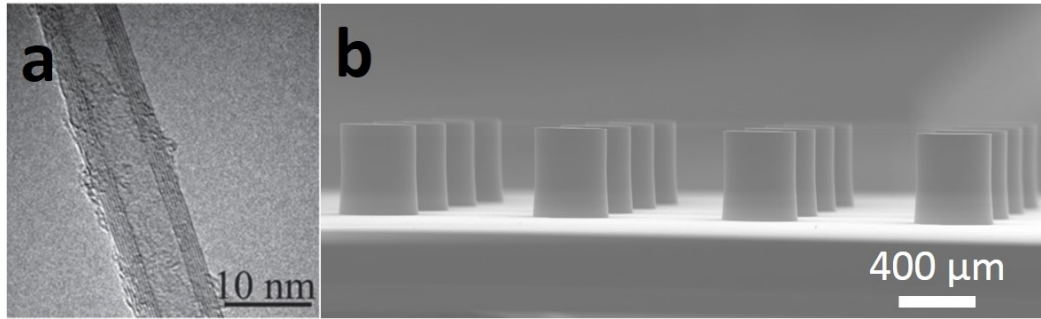


Figure 2.2: (a) TEM picture of one typical multi-wall CNT. (b) SEM picture of one typical CNT bundle array. Both samples were grown by the CVD method.

iron, copper or cobalt, at a temperature between 500°C and 1000°C. This method generally involves the dissociation of the hydrocarbon molecules and the saturation of the carbon atoms in the catalyst metal nano-particles. The precipitation of carbon from the saturated metal particles leads to the formation of the CNTs. Additional hydrogen or ammonia gases are used for the activation and reactivation of the catalytic surface. The CVD method usually produces lower quality CNTs compared with the other two methods. But in return, the CVD method has a higher production rate and more freedom of controlling the resultant CNT bundles' geometry, as the catalyst particles can be easily patterned and the synthesis environment can be precisely conditioned.

The characteristics of different CNT growth methods are summarized by reference [49] and briefed in Table 2.1. In this thesis, the randomly dispersed CNTs in Paper E were produced by the external supplier, while all the other vertically aligned CNTs were synthesized by the in-house CVD machine. Figure 2.2a shows the transmission electron microscopy (TEM) picture of one typical multi-wall CNT produced by the CVD method. Figure 2.2b shows the scanning electron microscope (SEM) picture of such CVD-grown CNTs in an array form.

3

TECHNOLOGY DEVELOPMENT

The processes required for handling emerging new materials like the CNTs are quite different from those of the traditional materials like metals or polymers. For instance, the technologies to process metals have been developed for hundreds of years. There are established process flows, such as welding, soldering, annealing, alloying, and plating, etc., to transform metals from one form to another. There are huge equipments to handle tons of metals, as well as dedicated equipments to produce thin metal films with atom-level thickness.

But for those recently discovered new materials like the CNTs, there are no established infrastructures. Those well-established process techniques cannot be simply adapted and applied. Instead, process innovations are required due to the unique physical, chemical and geometrical properties of the CNTs. New process flows need be devised and new equipments need be built, in order to properly manipulate and transform the CNTs according to various application requirements.

This chapter describes the detailed methods for the synthesis, densification, transfer, coating and composite formation of the CNTs for interconnect applications.

3.1 CHEMICAL VAPOR DEPOSITION OF CARBON NANOTUBES

A commercially available CNT CVD machine¹ is used for the in-house growth work in this thesis (Figure 3.1).

There are two widely accepted growth modes for CVD CNTs: tip growth and base growth (Figure 3.2a, b). Both modes are based on the vapor-liquid-solid theory developed by Wagner and Ellis [51]. In their model, hydrocarbon gases are decomposed, dissolved and supersaturated in the catalyst particle. Carbon diffuses through the catalyst particle and gets precipitated from the solution, thus forming the walls of the nanotubes. The catalyst-substrate interaction is found to play a dominant role for the difference in growth modes. Weak interaction, which is indicated by a larger catalyst-substrate contact angle (Figure 3.2a), tends to yield tip-growth CNTs, whereas strong interaction, indicated by a smaller contact angle, tends to yield base-growth CNTs (Figure 3.2b). Reference [52] provides an insightful review of the catalytic growth of CNTs by the CVD method.

¹ Black Magic, AIXTRON SE

3.1 CHEMICAL VAPOR DEPOSITION OF CARBON NANOTUBES

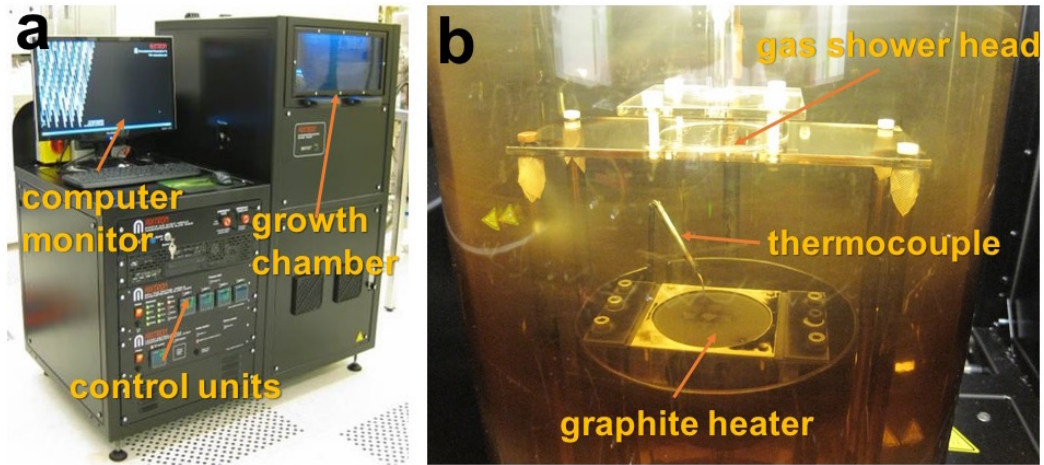


Figure 3.1: (a) The Black Magic machine from AIXTRON. (b) The quartz growth chamber inside the Black Magic.

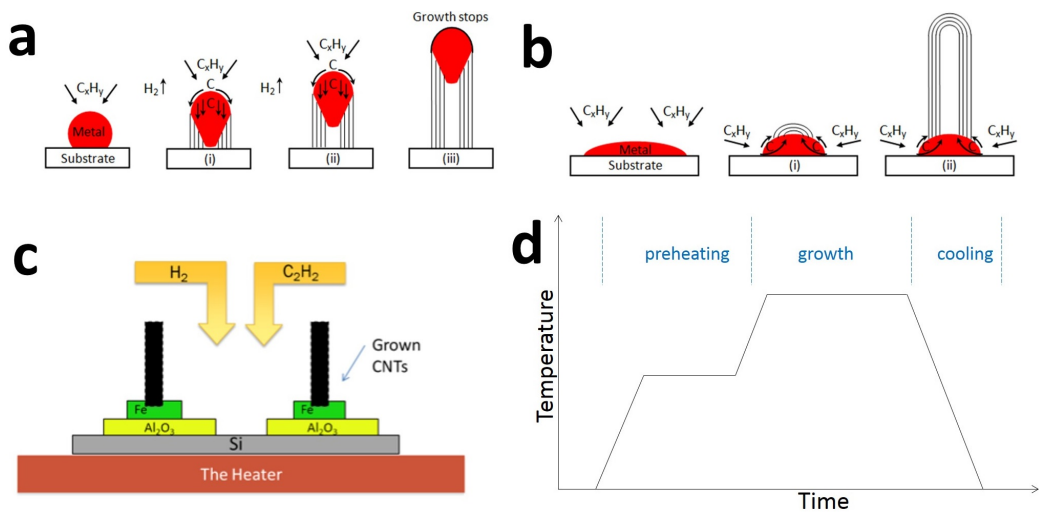


Figure 3.2: Widely accepted CNT CVD growth mechanisms. (a) Tip Growth. (b) Base Growth. (c) Gases and catalysts used in this thesis. (d) A typical temperature profile of a complete CNT growth cycle. Temperature measured on the surface of the graphite heater. (figure a, b adopted from reference [50])

3.1 CHEMICAL VAPOR DEPOSITION OF CARBON NANOTUBES

Parameter	Typical value	Tunable range
Catalyst thickness (iron)	1 nm	1 - 5 nm
Barrier layer thickness (alumina)	10 nm	> 5 nm
Preheating time	180 sec	180 - 300 sec
Preheating temperature	500°C	500 - 550°C
Growth time	8 min	1 - 10 min
Growth temperature	700°C	650 - 850°C
H ₂ gas flow	698 sccm	600 - 850 sccm
C ₂ H ₂ gas flow	200 sccm	150 - 250 sccm

Table 3.1: Typical growth conditions and corresponding tunable ranges of the thermal CVD method used in this work.

A simplified illustration of the growth environment configuration used in this thesis is depicted in Figure 3.2c. The substrate is patterned using standard photolithography with 10 nm alumina under 1 nm iron as the barrier/catalyst film structure. The alumina film helps to prevent the iron catalyst from diffusing into the silicon substrate. After the iron and alumina films are patterned, the sample is loaded on a graphite heater in the quartz growth chamber of the Black Magic (Figure 3.1b). The chamber is pumped down to below 0.2 mbar to create a sufficient vacuum. A generalized growth temperature profile of the heater is shown in Figure 3.2d. In the first stage, called preheating, the heater rises up to 500°C while controlled amount of hydrogen (H₂) gas is fed into the chamber. The chamber is kept at 500°C for up to 3 minutes. Right after the preheating follows the growth stage, in which the temperature of the heater is raised up to above 700°C and acetylene (C₂H₂) gas is fed into the chamber as soon as the temperature starts to rise. The growth stage time is adjusted according to the required length of the grown CNTs. The typical growth rate is around 100 μm/min given the typical parameters listed in Table 3.1. This growth rate holds true until the length of CNTs reach around 250 μm to 300 μm, after which the growth gets saturated and the rate slows down. To finish the growth, the whole chamber is cooled down by 1000 sccm nitrogen flow before the sample is taken out. The CNTs just taken out of the growth chamber will be referred to as the “pristine CNTs” or “raw CNTs” in the rest of this thesis, differing from the “densified” or “transferred” CNTs that are further processed.

Table 3.1 lists the important growth parameters, their typical values and tunable ranges for the thermal CNT CVD process. The growth result is dependent on several key factors which are discussed as follows.

3.1 CHEMICAL VAPOR DEPOSITION OF CARBON NANOTUBES

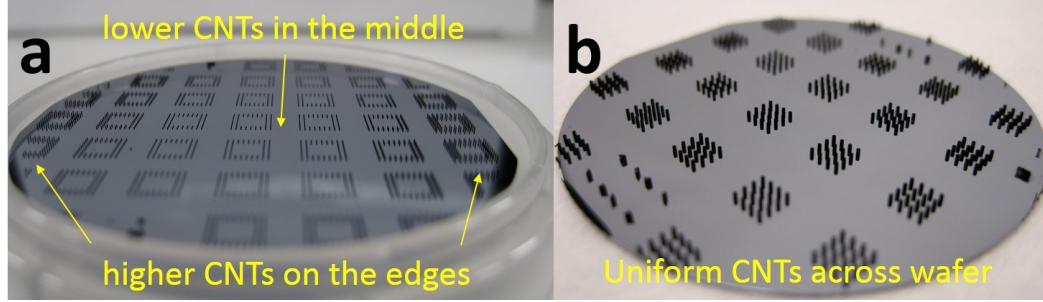


Figure 3.3: The uniformity issue caused by different gas flow rates. (a) Non-uniform growth on a 2-inch wafer due to the insufficient gas supply. The edge CNTs are higher than those in the center. (b) Uniform growth on a 2-inch wafer after increasing the gas flow.

3.1.1 *Impact of H_2 and C_2H_2 Flow Rate*

The original flow rates of H_2 and C_2H_2 are 698 sccm and 200 sccm, respectively, according to the suggestion from the vendor of Black Magic. It works well on small-sized samples (up to $9\text{ mm} \times 9\text{ mm}$), but not always on larger 2-inch silicon wafers. Figure 3.3a shows the growth result on a 2-inch wafer using 698 sccm/200 sccm H_2/C_2H_2 . It can be clearly observed that the CNT bundles in the wafer center are much shorter than those in the edge areas (the word bundle and forest are used interchangeably in this thesis to describe CNTs structures grown by patterned iron catalyst). The growth becomes uniform after increasing the gas flows to 830 sccm/240 sccm H_2/C_2H_2 , as shown in Figure 3.3b. Our hypothesis is that the 698 sccm/200 sccm flow rate generated non-uniform gas concentration on the surface of the wafer, thus causing uneven growth. Due to the difficulties in probing the gas flow pattern in real time, a definitive conclusion cannot be given at this moment.

3.1.2 *Impact of Bundle Aspect Ratio*

The structural quality of the CNT growth is dependent on the length of the CNT bundles. Figure 3.4a is the SEM graph of the growth result of two $1\text{ }\mu\text{m} \times 5\text{ }\mu\text{m}$ CNT bundles sitting on top of two molybdenum electrodes, using the typical growth conditions listed in Table 3.1. The bundles were grown to a height of $15\text{ }\mu\text{m}$, which resulted in an aspect ratio of around 15:1. Another growth result of the same catalyst and barrier layer configuration is shown in Figure 3.4b, but in this case the bundles are more than $100\text{ }\mu\text{m}$ high instead, giving a more than 100:1 aspect ratio. It is clear that the longer CNTs became distorted and started to curve at the later stage of the growth. This result infers that the CNTs with higher aspect ratios are vulnerable to structural distortion at later stages of the growth.

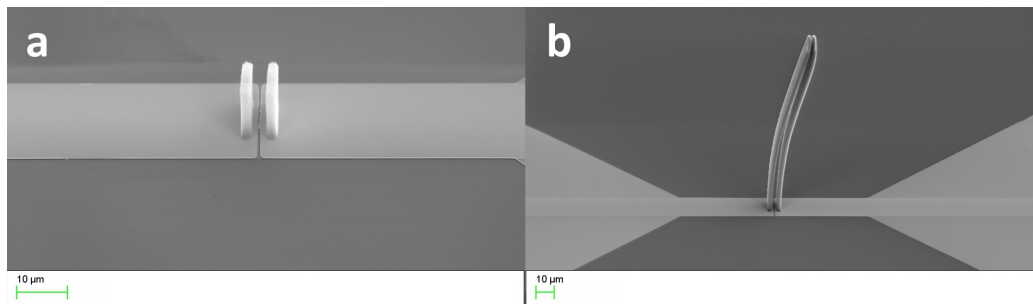


Figure 3.4: SEM micrograph of the CNT bundles of different aspect ratios. (a) Two $1\ \mu\text{m} \times 5\ \mu\text{m}$ CNT pillars grown for $15\ \mu\text{m}$ long. (b) The same pattern grown for more than $100\ \mu\text{m}$ long.

3.2 DENSIFICATION OF CARBON NANOTUBES

Pristine CVD-grown CNT forests are porous. During the last decades, many attempts have been made to increase the volume fraction of the CVD-grown CNT forests. Catalyst engineering has been employed to increase the nanoparticle density [53, 54], but the CNT forests produced by these methods are still much less dense than the ideally packed ones. Post-growth densification methods have also been developed. Mechanical compression was proposed to densify the CNTs by applying an external force on the CNT forests [55, 56]. Immersion of the CNTs into liquid was used to achieve a wet densification using capillary force [57, 58]. Vapor instead of liquid was later introduced in the wet method, which improved the quality of the densified CNTs [59]. A dry method was also developed, based on encapsulating CNTs at low pressures [60]. Judging from all of these reported works, vapor densification seems to produce the best results in terms of uniformity and stability.

3.2.1 Vapor Densification Method

A detailed study of the vapor densification method has been carried out within the scope of this thesis (Paper A). Figure 3.5a, b show the experimental setup and the corresponding result of a vapor densification method. A chip carrying raw CNT forests was placed on a lid above a beaker containing a boiling solvent. The solvent used here was acetone diluted in water, heated to 75°C . Other evaporative solvents, such as isopropanol and methanol, were also proven to be able of delivering similar densification results. The entire vessel was closed. After the sample was taken away from the beaker and cooled down, the solvent evaporated again leaving the individual CNTs drawn into each other by the capillary force in between. Longer exposure time led to more solvent condensed on the chip, hence generating more densified forests. It is clearly shown that the CNT forest structures are well-

3.2 DENSIFICATION OF CARBON NANOTUBES

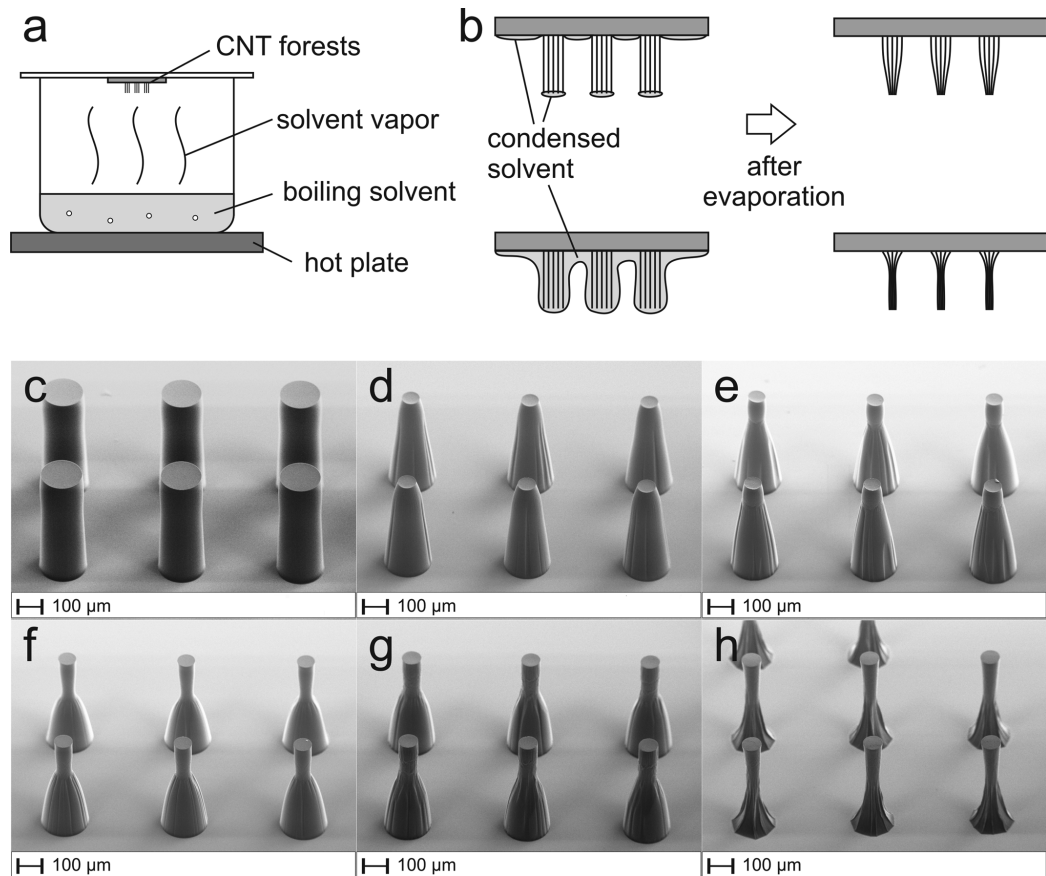


Figure 3.5: Formation of three-dimensional carbon nanotube structures by controllable vapor densification. (a) Illustration of the experimental setup of the vapor densification. The chip carrying CNT forests was placed on a lid above the boiling solvent, collecting controllable amount of solvent. (b) Illustration of the mechanism of the vapor densification. After collecting and evaporating different amounts of solvent, the CNT forests can be densified to different degrees. (c) Undensified CNT forests. (d-h) CNT forests densified after exposing to the solvent vapor for 20 (d), 30 (e), 40 (f), 50 (g), and 60 (h) seconds. (from Paper A)

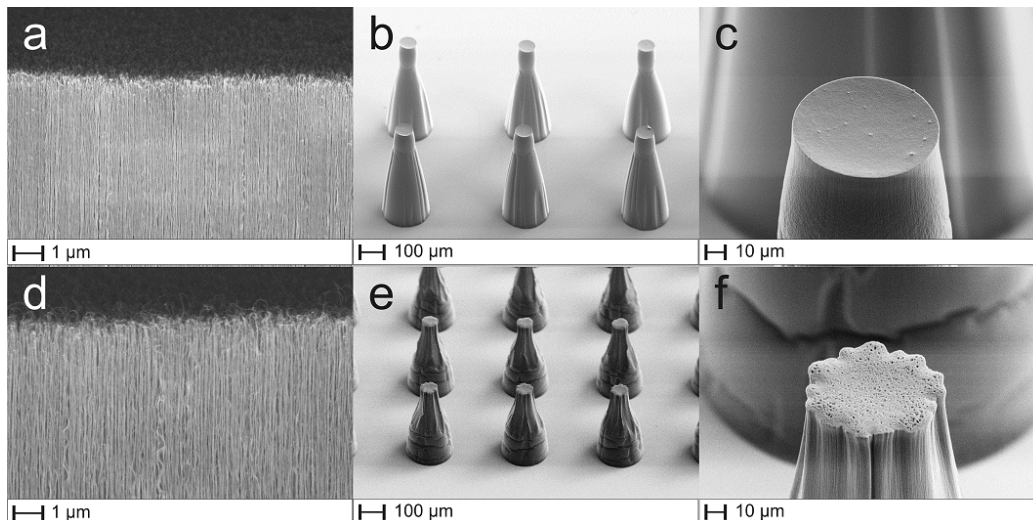


Figure 3.6: Densification results of CNT forests with different volume fractions. (a-c) CNT forests grown at an pre-heating temperature of 500°C. (d-f) CNT forests grown at an pre-heating temperature of 600°C. (from Paper A)

preserved, thus further manipulation of such densified bundles is possible (Figure 3.5c-h).

The densification result is affected by the site density of the raw CNT forests. CNTs of different volume density are prepared by varying the pre-heating temperature and densified with vapor densification method. Higher pre-heating temperature (600°C) produces bigger and sparser iron catalyst particles while lower temperature (500°C) produces smaller and denser particles. For forests with high CNT density, their original shape (circular in this case) is maintained after the densification (Figure 3.6a, b, and c). For more porous CNT forests, their original shapes are distorted after densification (Figure 3.6d, e and f).

3.2.2 Paper-Mediated Wet Densification Method

Although the vapor densification method described above produces high quality densified CNT bundles, the control of the vapor can be difficult when dealing with micro- or nano-sized structures at larger scales. Therefore, densification on a large substrate, i.e. on silicon wafers, cannot be well controlled by this method. In order to further improve the densification of the CNTs, a paper-mediated wet densification method has been developed (Paper C). Figure 3.7 shows the illustration of an improved wet densification method based on the previously discussed vapor densification. A piece of paper wet with acetone was used as the liquid source instead of the boiling acetone-water mixture. The paper-mediated densification process was set up by wetting a piece of paper at room temperature using acetone, and putting the raw CNT-carrying silicon substrate upside down onto that wet paper. When the CNT forests were in contact with the wet paper surface, the capillary force

3.2 DENSIFICATION OF CARBON NANOTUBES

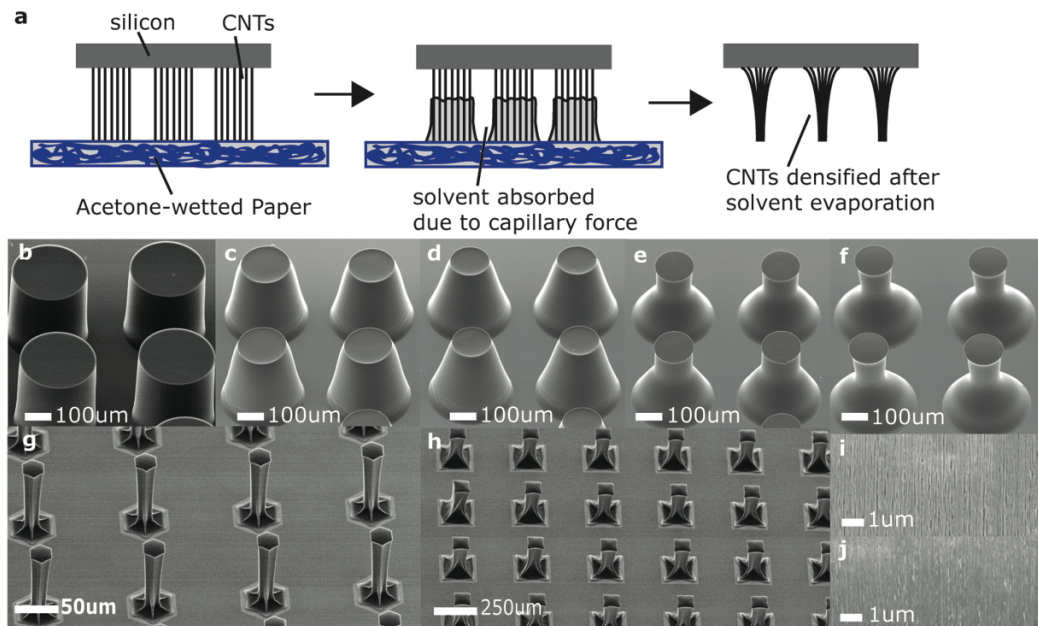


Figure 3.7: Paper-mediated liquid densification process of the CNT forests. (a) Illustration of the experimental setup and the mechanism of the paper-mediated densification. (b) Undensified CNT forests. (c-f) Densification result after contacting the paper surface for 15(c), 30(d), 45(e), 120(f) seconds. (g) Hexagon-shaped CNT forests after densification. (h) Square-shaped CNT forests after densification. (i-j) High magnification SEM micrograph of the sidewalls of the CNT forests before (i) and after (j) the densification. (from Paper C)

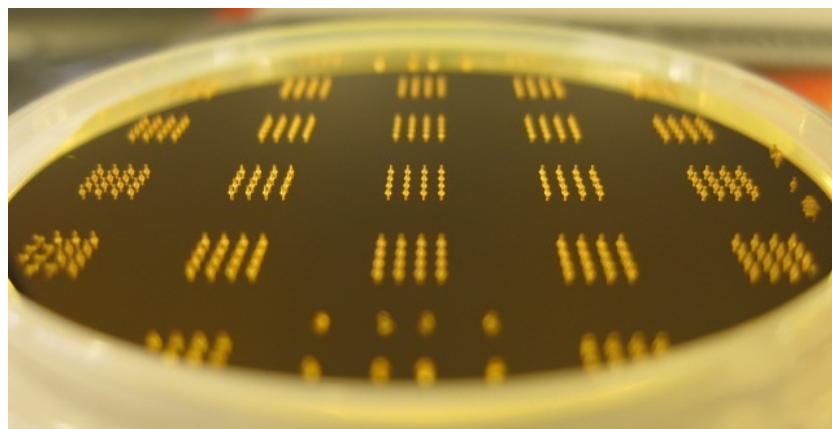


Figure 3.8: Densification of CNTs on a 2-inch wafer. The CNTs are sputter-coated with titanium and gold.

	Un-densified (μm)	Densified (μm)
Average height	523.6	368.6
Standard deviation	1.4	3.5
Maximum height	527.6	375.6
Minimum height	521.5	358.7

Table 3.2: Heights of one un-densified and one densified array of 8×8 CNT forests densified by the vapor densification method. (from Paper A)

	Un-densified (μm)	Densified (μm)
Average height	400.6	394.1
Standard deviation	1.2	4.9
Maximum height	402.7	399.2
Minimum height	390.9	380.8

Table 3.3: Heights of one un-densified and one densified array of 8×8 CNT forests densified by the paper-mediated densification method. (from Paper C)

drove the acetone up along the gaps between individual CNTs. The surface tension thereby collapsed the loosely porous CNT forests into densely packed bundles. After removing the substrate from the paper, the acetone evaporated and densified CNT bundles were hence formed. The degree of densification can be controlled by limiting the contact time of this self-assembly process. This paper-mediated densification method generates similar results as the vapor densification method. Being an improvement, this paper-mediated method increases the stability of the process as trapped liquids are much easier to control than the vapor from the boiling liquid. Wafer level densification can thus be achieved, which greatly improves the scalability of the densification process (Figure 3.8).

3.2.3 Height Uniformity of Densified Carbon Nanotubes

The height uniformity of the densified CNT arrays, resulting from the above two densification methods, has been carefully characterized. Two sample substrates, each containing 8×8 CNT forests, were prepared in the same batch, one densified and the other not, were measured using the contact-less optical surface profiler².

Table 3.2 and Table 3.3 compare the CNT uniformity before/after the vapor and the paper densification methods, respectively. In Table 3.2, the raw CNT forests

² Interferometer Wyko NT1100, Veeco Instruments Inc.

3.2 DENSIFICATION OF CARBON NANOTUBES

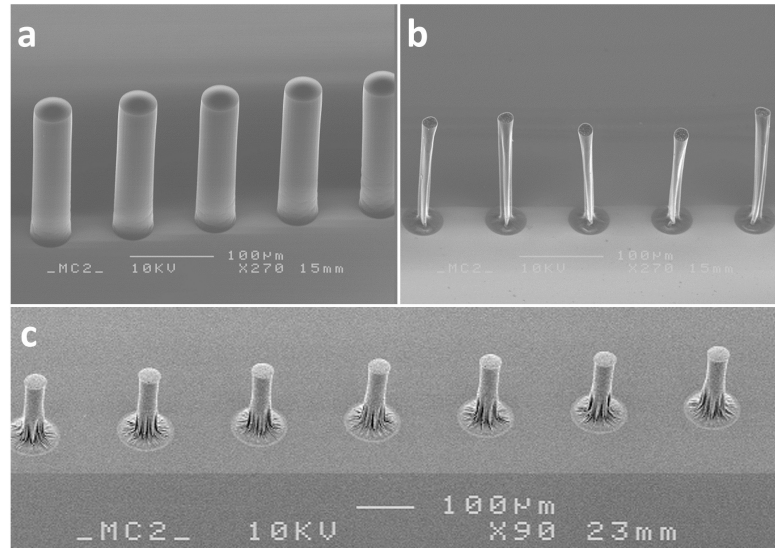


Figure 3.9: Impact of the aspect ratio on the quality of densification. (a) Longer CNT forests before densification. (b) Longer CNT forests after densification. (c) Shorter CNTs of same diameter get better densification quality.

are highly uniform, the standard deviation being lower than 0.3% of the average height. The vapor densification process only slightly deteriorates the uniformity. The standard deviation of the forest heights is lower than 1% of the average height after densification. Heights of the tallest and shortest forests are both within $10\ \mu\text{m}$ from the average value, $368.6\ \mu\text{m}$. Similarly in Table 3.3 for the paper densification method, with the average height decreased from around $400\ \mu\text{m}$ to $394\ \mu\text{m}$ due to densification, the standard deviation only slightly increased from 0.2% to 1.2%. Both densification methods exhibit good quality in terms of uniformity.

3.2.4 Impact of Bundle Aspect Ratio

The quality of densification was also found to be dependent on the aspect ratio of the CNT bundles. Figure 3.9 shows the comparison of the densification results of high and low aspect ratio CNT bundles. High aspect ratio cylindrical CNTs were grown (Figure 3.9a) and densified using the vapor densification method (Figure 3.9b). To compare, CNT forests of similar diameter were grown for shorter length and densified using the same method (Figure 3.9c). It can be clearly seen from these figures that the shorter CNTs receive much more uniform densification result than the longer ones. The aspect ratio for producing distortion-free densified cylindrical CNT bundles was found to be between 2:1 to 4:1. As the densification will reduce the diameter of the bundles to around $1/3$ of the origin (Paper A and C), the resulting densified CNTs can have an aspect ratio of more than 6:1 with good quality control.

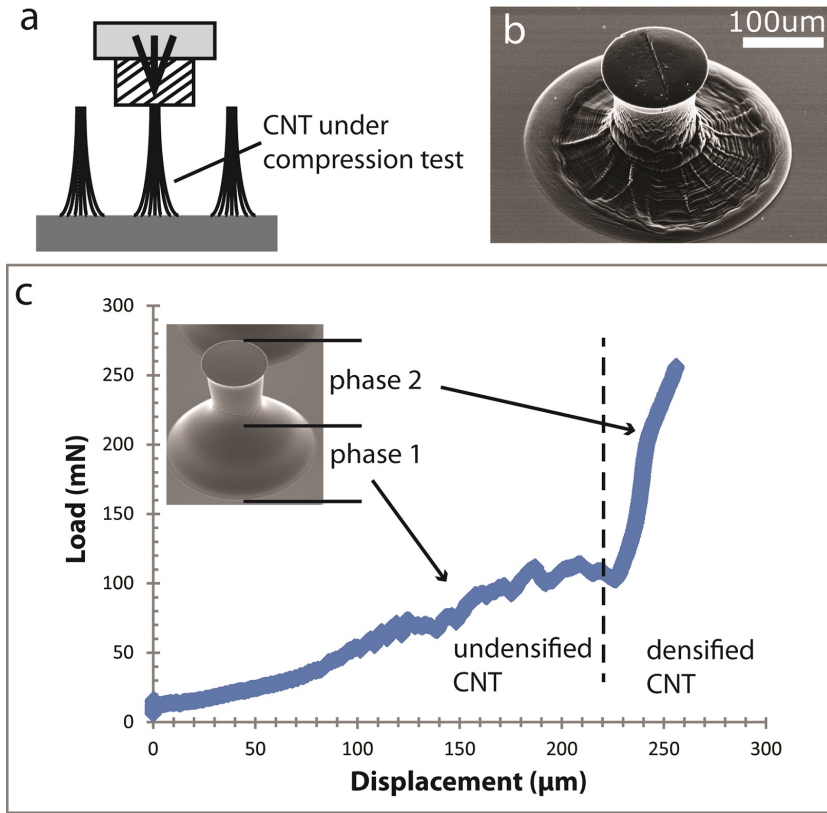


Figure 3.10: (a) Illustration of the compression test on the densified CNT bundles. (b) SEM micrograph of one partially-densified CNT bundle after compression test. (c) Plot of the load versus displacement measurement of one partially-densified CNT bundle. Two phases of the compression can be distinguished by the change of slope near 230 μm displacement. (from Paper C)

3.2.5 Young's Modulus of CNT Bundles

By controlling the densification time, we are able to stop the densification at the degree that dual-porosity vertically aligned CNT structures similar to those made by Futaba et al. [61] were produced (Paper C). The strength of the as-densified bi-phase CNT bundles was tested by compressing the structure in the vertical direction and measuring the corresponding load versus displacement curve (Figure 3.10a). The CNT forest used in this test was around 400 μm in height and partially densified, which means some of the structure was left undensified (Figure 3.10c inset). One example of the measured load-displacement curve is shown in Figure 3.10c and the CNT bundle after compression test is shown in Figure 3.10b. Due to the dual-porosity of the structure, the load-displacement curve can be divided into two phases, of which the first phase corresponds to the deformation of the undensified section and the second phase to that of the densified one. Six samples were tested in this experiment and the calculated Young's modulus of the

3.3 TRANSFER OF CARBON NANOTUBES

undensified section is approximately $15.8 \text{ MPa} \pm 2.5 \text{ MPa}$ on average, which is similar to the results of the previous studies [62]. In the second phase of the tests, the Young's modulus increased to approximately $111.9 \text{ MPa} \pm 45.7 \text{ MPa}$ for the densified CNT part, leading to a significant enhancement of the material strength. The observation of two distinct modulus phases is similar to the finding of J. Suhr et al. [63], in which the densification of the CNTs are achieved by the compression test itself.

3.3 TRANSFER OF CARBON NANOTUBES

Transfer technologies are introduced to relocate the raw CNTs from the growth substrate onto the target device substrates, in order to avoid exposing the target substrate directly to the high temperature ($>500^\circ\text{C}$) CVD synthesis environment, which is unacceptable for most existing devices. By using the transfer technology, CNT growth can be conducted at any arbitrary optimized conditions, and the target device surface can be chosen from a large variety of materials. Transferring CNTs thus brings the freedom of wider process flexibility. The first CNT transfer experiment was demonstrated by Huang et al. in 1999 [64], who showed that a CNT-carrying substrate was removed by immersing the nanotube-deposited quartz plates into an aqueous hydrofluoric acid solution and stand-alone CNT films were obtained. Since this kind of solution-based wet method has difficulties in controlling the shape and uniformity of the CNTs arrays, a lot of researchers now focus on the dry methods instead, which involves the use of assembly materials, such as solders and adhesives, for the transfer purpose [65–68].

The choice of transfer material and process is highly dependent on the requirement of the application. In applications where high electrical conductivity is required, solder metals [68–73] or conductive adhesives [74, 75] are mostly studied for the transfer process. In applications where structural integrity is desired, non-destructive transfer processes using curable polymers are preferred. The merits and limitations of different transfer methods and processes are discussed in the following sections.

3.3.1 *Transfer by Indium*

Metal is the mostly widely adopted interconnect material in electronics. Thus the use of metal for transferring the CNTs are quite natural [68–73]. One commonly used metal is indium (In) due to its low melting temperature [68]. Figure 3.11 illustrates an example of the indium transfer process developed within the scope of this thesis (Paper B, C). The CVD-grown CNTs were sputter-coated with a layer of titanium and gold (Figure 3.11a) and then pressed onto a target substrate coated with a indium film (Figure 3.11c). The sample was then heated up to melt the indium (Figure 3.11d). After the indium was melted and alloyed with the titanium/gold film, the CNT growth substrate was removed and the CNTs were

3.3 TRANSFER OF CARBON NANOTUBES

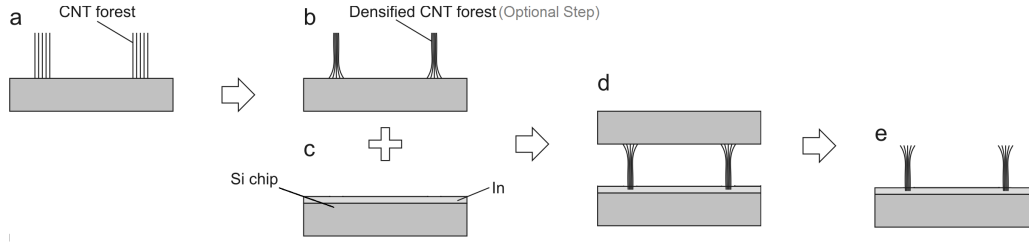


Figure 3.11: Illustration of the transfer process of the CNT forests using indium as the transfer medium. (a) Vertically-aligned CNT forests are grown and coated with a thin layer of titanium/gold. (b) The CNT forests are densified through a densification process (optional step). (c) The target chip is prepared with a thick indium layer (around $1\ \mu\text{m}$). (d) The two chips in (b) and (c) are aligned and then bonded at an elevated temperature (between 150°C and 200°C). (e) The growth substrate is separated.

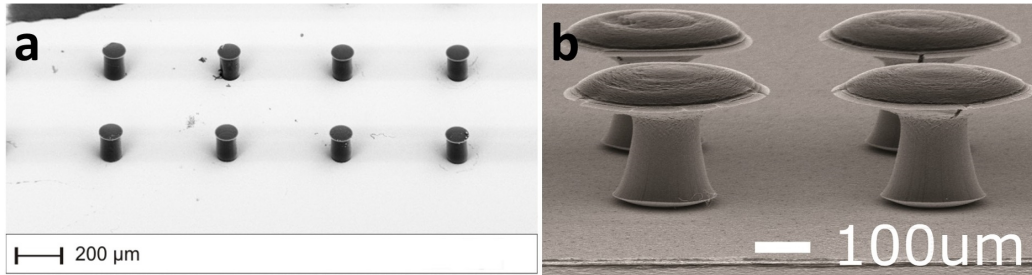


Figure 3.12: Indium-transferred CNTs. (a) Un-densified CNTs. (reference [76]) (b) Densified CNTs. (from Paper C).

therefore transferred (Figure 3.11e). This indium transfer technology can be used on both un-densified and densified CNTs (Figure 3.12a, b). In the attached paper B and C, the uses of indium as an transfer material for fabricating through silicon vias and interconnect bumps are described in detail. This process can be adapted to use conductive adhesives instead of indium in cases where temperature and pressure should be limited, as the curing of conductive adhesives usually requires lower temperature and the viscosity of the adhesives allows lower pressing force to ensure good contact with CNT bundles [67].

3.3.2 Transfer by Polymer

Although solders and adhesives have been widely studied for transferring the CNTs, the patterning and placement of solders or adhesives can be an unnecessary process overhead when CNTs are used specifically for wafer-level 3D interconnect, because solders and adhesives are rarely used at this stage of semiconductor fabrication. Furthermore, the process stability is still unsatisfactory due to the limited contact area with the CNT arrays. In Paper D, a new transfer process has been developed and implemented for integrating the CNTs as 3D through silicon vias (TSVs).

3.3 TRANSFER OF CARBON NANOTUBES

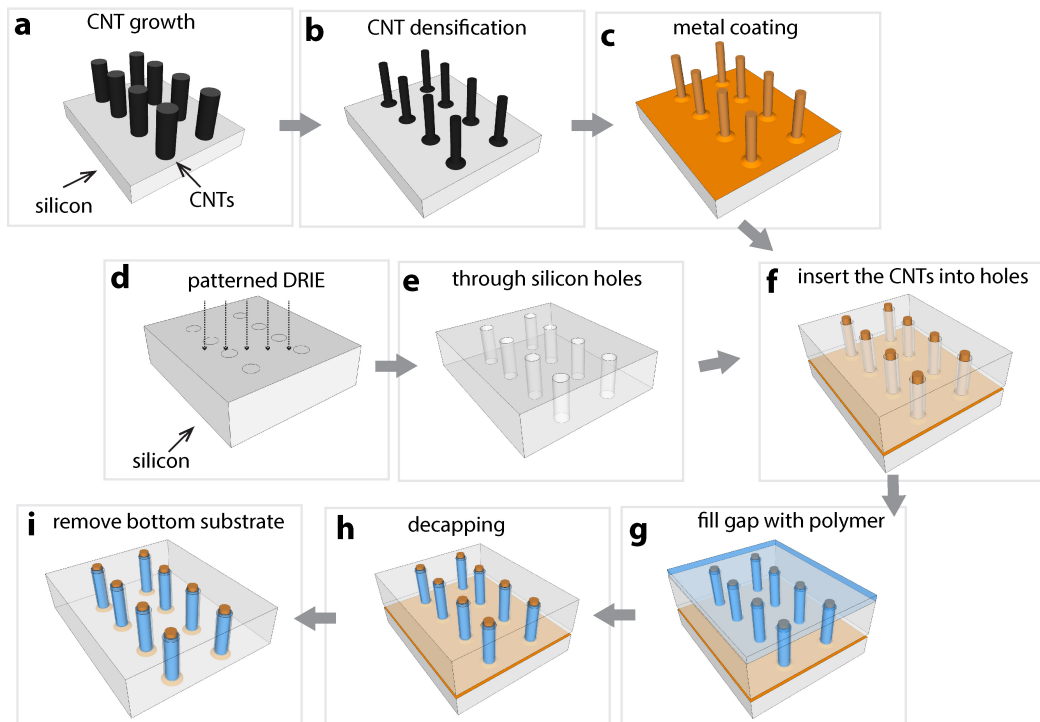


Figure 3.13: Fabrication process flow for transferring CNTs into silicon vias. (a) Growth of the CNTs on the silicon wafer. (b) Densification of the CNTs. (c) Coat the CNTs with titanium/gold layer. (d) Another silicon wafer patterned by DRIE. (e) Use DRIE to etch through the silicon wafer. (f) Align and insert the CNT wafer into the TSV wafer. (g) Fill the gaps between the CNTs and the via walls using BCB. (h) Use O_2 plasma etching to remove the BCB on CNT caps. (i) Remove the CNT growth wafer by DRIE. (from Paper D)

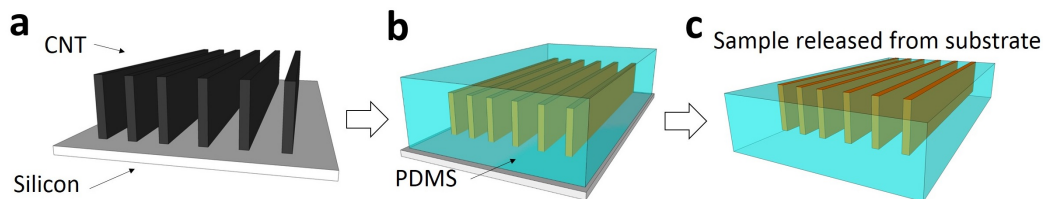


Figure 3.14: Illustration of the PDMS transfer method. (a) CVD CNT forests grown on silicon. (b) The sample, with or without metallic coating on the CNTs, is infiltrated with PDMS and cured. (c) The CNT/PDMS composite structure is released from the substrate, forming a free standing flexible film. (from Paper F)

Figure 3.13 is an illustration of the CNT transfer flow for filling the via holes. The CNTs were grown on a 2-inch silicon wafer. Next, the CNT-carrying wafer was densified using the paper-mediated densification method (Figure 3.13b). The CNT-carrying wafer was then coated with a titanium/gold layer by sputtering (Figure 3.13c). At the same time, a TSV wafer was prepared using standard photolithography and deep reactive ion etching (DRIE) (Figure 3.13d, e). The two wafers were then aligned using a flip-chip bonder³, and the CNTs were inserted into the through silicon holes (Figure 3.13f). In order to form a reliable bond between the CNTs and the TSV wafer, the joined wafers were spin-coated with a thin layer of benzocyclobutene (BCB) and cured at 250°C in nitrogen gas to fill the gaps between the CNTs and the via walls (Figure 3.13g). After the BCB was cured, the sample was put into a plasma etching chamber and etched by oxygen plasma at 250 W power for 7 minutes (Figure 3.13h). This plasma etching removed the BCB from the tips of the CNT bundles, exposing the CNTs for electrical contact for the further processing, and therefore creating a through silicon path from the bottom to the top side of the TSV wafer. Finally, the substrate carrying the CNTs was removed by etching from the backside, so that the silicon wafer with transferred CNT TSVs was completed (Figure 3.13i). We also tried out two polymers other than BCB, i.e. polymethyl methacrylate (polymethyl methacrylate (PMMA), 11% solid in anisole) and epoxy resin. It was observed that polymers with lower viscosity (BCB, epoxy resin) generated better transfer results than the highly viscous 11% PMMA.

This transfer method was further modified, using silicone-based polydimethylsiloxane (PDMS) instead of BCB, for the fabrication of CNT/polymer composite material. In this modified process, PDMS solution was poured onto the vertically aligned or randomly dispersed CNTs, with or without metallic coating depending on the application (Figure 3.14a, b). Next, the sample was put into vacuum below 50 mbar to remove the bubble inside the PDMS. After de-bubbling, the sample was put stationary in a refrigerator at 10°C for over 5 hours to allow complete infiltration of PDMS into the CNT network. Afterwards, the sample was heated up to 80°C for 20 minutes to cure the PDMS. Once the PDMS was cured, it formed

³ FINEPLACER® lambda, Finetech GmbH

3.4 METALLIC COATING OF CARBON NANOTUBES

a composite with the CNTs and the composite film could be easily removed from the underlying substrate, resulting in a flexible sheet with patterned CNTs fully embedded (Figure 3.14c). This process has been used in the CNT-based flexible interconnect applications which are further described in Paper E, F and G.

3.4 METALLIC COATING OF CARBON NANOTUBES

There have been numerous studies on the metallic coating technologies for the CNTs. Although experimental works have shown the great electrical and mechanical properties of the raw CNTs, it still remains a challenge to produce large quantities of CNTs with the reported excellence in electron transport and mechanical strength. The relatively low synthesis temperature of the CVD method implies insufficient energy input as compared with the laser or arc discharge methods, which are capable of producing CNTs with record properties [6, 7]. However, as is discussed in the last chapter, CVD is the only method that produces well-patterned and aligned CNT arrays. This makes it particularly favorable in electronics applications where the control of geometry is essential to make any functional devices. Furthermore, pristine CNTs usually form poor contact with metals due to the existence of Schottky barriers [77]. This severely hinders the possibility to use CNTs to improve existing electronic devices.

In this thesis work, two types of metallic coating techniques, one for the aligned directional CNTs and the other for the randomly dispersed CNTs, have been developed and characterized.

3.4.1 *Sputtering and Electroplating Metals on Carbon Nanotubes*

Titanium is reported to be one of the most suitable contact metals for the CNTs [78, 79]. It can be easily deposited onto the CNTs either by sputtering or by evaporation. Due to the high aspect ratio nature of the CNT bundles used in this thesis, sputtering is more preferable as it offers better side wall coverage. It is also possible to sputter additional metal layers after the titanium deposition for various purposes. For example, aluminum can be used to increase the conductivity of the CNTs because it is cheap and highly conductive. Gold is often used as the passivation and protection layer against the ambient environment. In this work, the surface morphology of the CNT bundles is studied by increasing the sputtered metal thickness. As shown in Figure 3.15, the metal layers start to coat individual CNTs and gradually form a continuous film as the gaps between the nanotubes are closed by the increasing amount of deposited metals. However, it should be noted that, the sputtered metal atoms cannot penetrate deep into the CNT bundle to coat the inner nanotubes. One CNT bundle coated with 20 nm/50 nm titanium/gold was intentionally destroyed to expose the inner structure (Figure 3.16a). The side view into the crack opening revealed that the sputtered titanium/gold stayed only on the bundle surface and the inner nanotubes were not coated (Figure 3.16b).

3.4 METALLIC COATING OF CARBON NANOTUBES

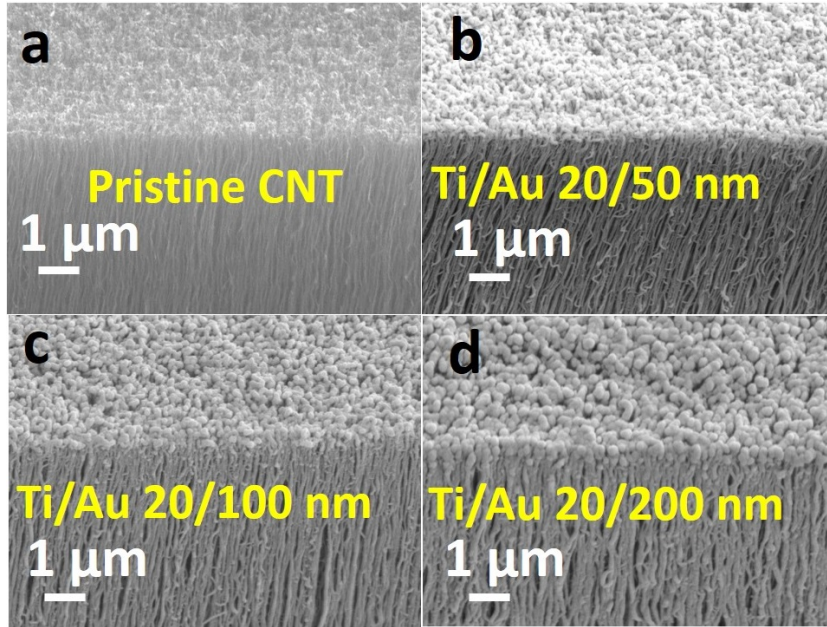


Figure 3.15: SEM micrograph of the surface morphology of the pristine and the metal-coated CNTs. (from Paper G)

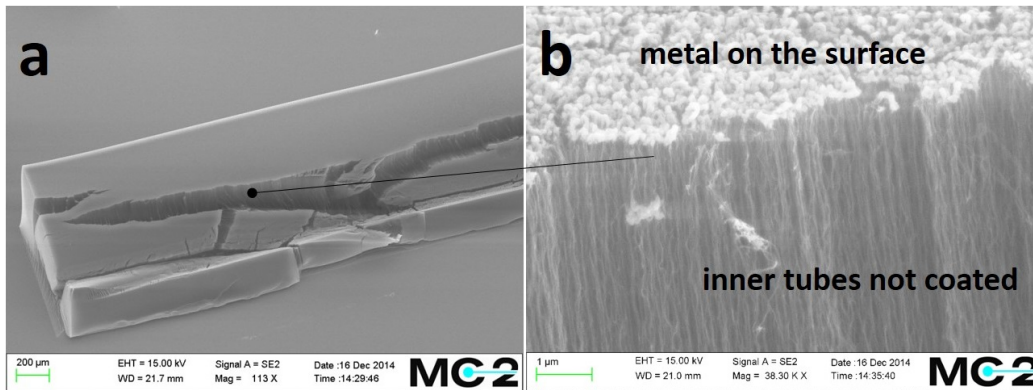


Figure 3.16: (a) One CNT bundle coated with titanium/gold was intentionally destroyed to expose the inner nanotubes. (b) The side view into the crack opening revealed that the sputtered metals stayed only on the bundle surface and the inner nanotubes were not coated.

3.4 METALLIC COATING OF CARBON NANOTUBES

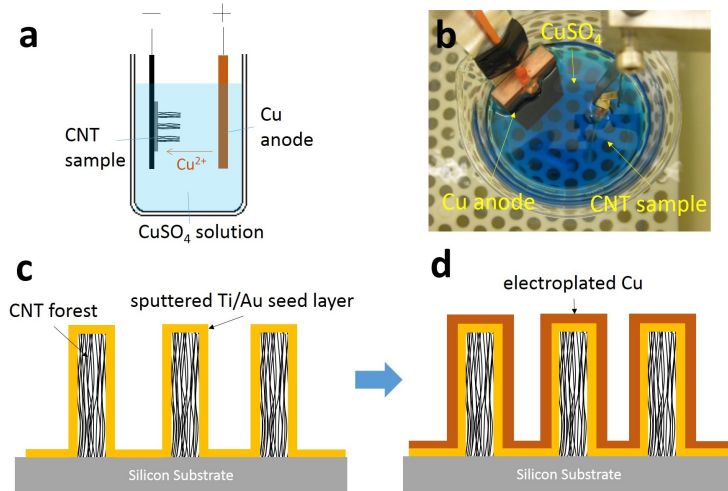


Figure 3.17: (a) Illustration of the copper electroplating apparatus setup. (b) Picture of the apparatus setup. (c) The CNT sample was sputter-coated with titanium/gold as the seed layer for electroplating. (d) Copper started to agglomerate on the CNT surface during plating.

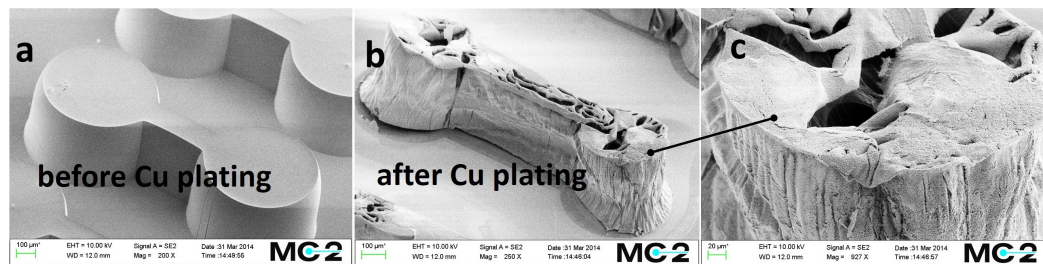


Figure 3.18: (a) SEM micrograph of the pristine CNT forest before copper electroplating. (b) The same CNT forest after 2-minute's copper electroplating. (c) Zoom-in picture on the copper/CNT surface.

The thickness of the sputtered metal is usually limited to several hundreds of nanometers. In order to obtain even thicker metal layers, electroplating can be used. In this work, copper electroplating on the CNT surfaces has been studied. The copper electroplating apparatus setup is illustrated in Figure 3.17a, b. The CNT sample was first sputter-coated with 20 nm/100 nm titanium/gold seed layer (Figure 3.17c). It was then put in the CuSO_4 solution (J-PLATE CU 400) and connected to the plating cathode. The copper source was connected to the anode. After the power supply was turned on, copper started to agglomerate on the CNT sample surface, driven by the electrical current through the Cu^{2+} -rich solution. The plating current was set to 2-3 A/dm^2 for optimal plating quality. The speed of copper plating was measured to be around $0.6 \mu\text{m}/\text{min}$.

The quality of copper plating was examined by SEM. Figure 3.18 shows the result of a 2-minute plating on a quite large CNT structure (features at millimeter scale). The comparison between the CNT structures before and after the plating

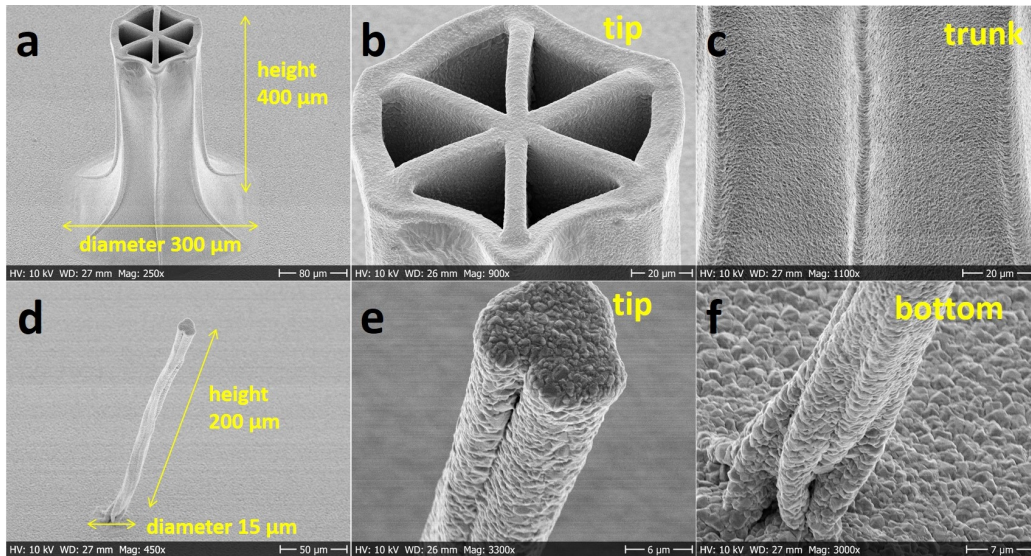


Figure 3.19: CNT copper electroplating results. (a) SEM micrograph of a hexagonally patterned CNT bundle, pre-densified and electroplated with copper for 2 minutes. (b) Zoom-in picture of the tip of the hexagonal CNT bundle. (c) Zoom-in picture of the trunk of the hexagonal CNT bundle. Uniform and continuous copper film was plated all over the CNT structure. (d) A hexagonally patterned CNT bundle produced by the same densification and electroplating process. (e) Zoom-in picture of the CNT tip, distorted and fully copper-covered. (f) Zoom-in picture of the CNT root and silicon substrate. Copper crystals with diameter of 1-2 μm can be clearly observed.

process clearly shows the formation of a continuous yet defective copper film on the CNT forest surface (Figure 3.18a, b). Due to the high porosity of the pristine CNTs, the immersion into the plating solution created significantly large voiding and distortion inside the bundle structures (Figure 3.18c).

By applying the densification process before copper electroplating, the structural integrity of the CNT forest can be retained thus improving the plating quality. Figure 3.19a-c contain the SEM micrographs of a hexagonally patterned CNT bundle, 300 μm in diameter and 400 μm in height, pre-densified and electroplated with copper for 2 minutes. The zoom-in pictures of the CNT tip and trunk (Figure 3.19b,c) show quite good copper film uniformity. No voiding or breakage could be observed. The same plating process was applied to even smaller CNT bundles with 15 μm in diameter and 200 μm in height (Figure 3.19d-f). For samples of such a large aspect ratio, the structural integrity could no longer be retained, thus leading to a distorted CNT bundle after electroplating. A 2-minute plating gave a copper film of around 1.4 μm in thickness which completely filled up the whole CNT structure. Copper crystals with diameters of 1-2 μm could be clearly observed on the surface of both the CNT and the silicon substrate (Figure 3.19e,f).

Four-probe measurement was carried out to characterize the resistance of the copper-plated CNT bundles. Figure 3.20 shows the I-V curve of a typical copper-

3.4 METALLIC COATING OF CARBON NANOTUBES

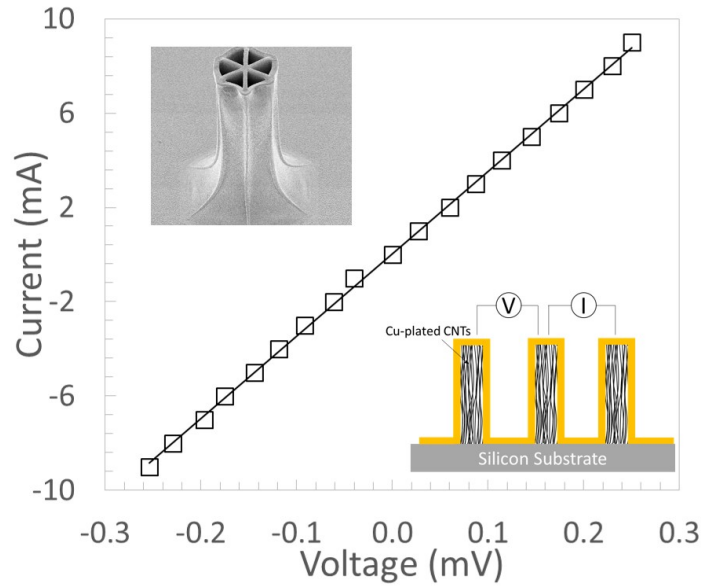


Figure 3.20: I-V curve of a typical copper-plated CNT bundle. The four probe measurement resulted in a resistance of $35\text{ m}\Omega$, which can be converted into resistivity of $6.9\times 10^{-7}\text{ }\Omega\cdot\text{m}$ if the CNT bundle was approximated as a cylinder of $100\text{ }\mu\text{m}$ in diameter and $400\text{ }\mu\text{m}$ in height.

plated CNT bundle. The resultant resistance was $35\text{ m}\Omega$, which can be converted into a resistivity of $6.9\times 10^{-7}\text{ }\Omega\cdot\text{m}$, if the CNT bundle was approximated as a cylinder of $100\text{ }\mu\text{m}$ in diameter and $400\text{ }\mu\text{m}$ in height. This resistivity is around two orders magnitude lower than that of the CNT bundles coated with titanium/gold layers of hundreds of nanometers thick (Paper C, D), and very close to the resistivity of widely used Sn-Ag-Cu solder alloys (around $10^{-7}\text{ }\Omega\cdot\text{m}$).

3.4.2 Solution Based Silver Coating on Carbon Nanotubes

Sputtering and electroplating provide good metal coverage on CNT bundles of large geometries. However, in certain cases, for example, CNT-based printing ink, complete metal coverage on individual CNTs is required. Therefore, a solution-based chemical coating process has been developed in this work to coat individual multi-wall CNTs with silver, aiming for the flexible interconnect applications. It must be noted that the credit for developing the following chemical coating process should be attributed to my co-worker, chemist Nan Wang. The details can be found in the attached paper E. In this thesis, the brief chemical process is included as a reference.

The fabrication processes of the CNT hybrid nanowires are schematically illustrated in Figure 3.21. The surface of the CNTs was successively coated with firstly a (3-Aminopropylaminopropyl) triethoxysilane (APTES) layer, then a silica layer, followed by palladium nanoparticle and silver nanoparticle deposition.

3.4 METALLIC COATING OF CARBON NANOTUBES



Figure 3.21: Schematic of the various modification steps in the synthesis of multi-functionalized CNT-based hybrid nanowires. The surface of CNTs was coated with APTES, silica, palladium nanoparticles, and silver nanoparticles. (from Paper E)

Every functional material in this process has been specifically chosen for its beneficial properties: CNTs act as a flexible framework as well as additional electron pathways. APTES improves the dispersion of CNTs in polar solvents by bringing in hydrophilic silane and amino groups on the surface of CNTs. The mesoporous silica layer is used as the template for the attachment and deposition of metallic nanoparticles. Palladium nanoparticles served as the catalyst to provide nucleation sites for silver growth. Silver nanoparticles are deposited in a silver nitrate solution and they are the main conductive media to improve the contact surface of the hybrid nanowires and to build high-efficiency conductive networks. Finally, functionalized CNT based hybrid nanowires were obtained through electroless silver plating.

To understand the morphology changes of the CNTs, TEM study was used before and after the silica coating process. The micrograph of the pristine CNTs shown in Figure 3.22a indicates a smooth CNT surface with a diameter of 10 nm. In comparison, a silica-around-CNT shell structure along the axial direction of the nanotubes can be observed from Figure 3.22b, which indicates a successful silica coating. The degree of silver nanoparticles coverage on the CNT surfaces was found to be very critical for optimizing the electrical performance of the hybrid nanowires. Hence, a series of functionalized CNT specimens were prepared with increased silver nitrate concentrations from 1 g/L to 15 g/L. TEM observation shows that the morphologies of the CNTs changed as the silver nitrate concentrations were varied (Figure 3.22c-f). When a lower silver nitrate concentration (1 g/L) was used, small silver nanoparticles with an average size of 20 nm were formed due to the absence of adequate silver precursor sources (Figure 3.22c). Upon increasing the concentration of silver nitrate from 1 g/L to 15 g/L, the average size of the silver nanoparticles was increased from 20 nm to 50 nm with better surface coverage (Figure 3.22c-e).

3.4 METALLIC COATING OF CARBON NANOTUBES

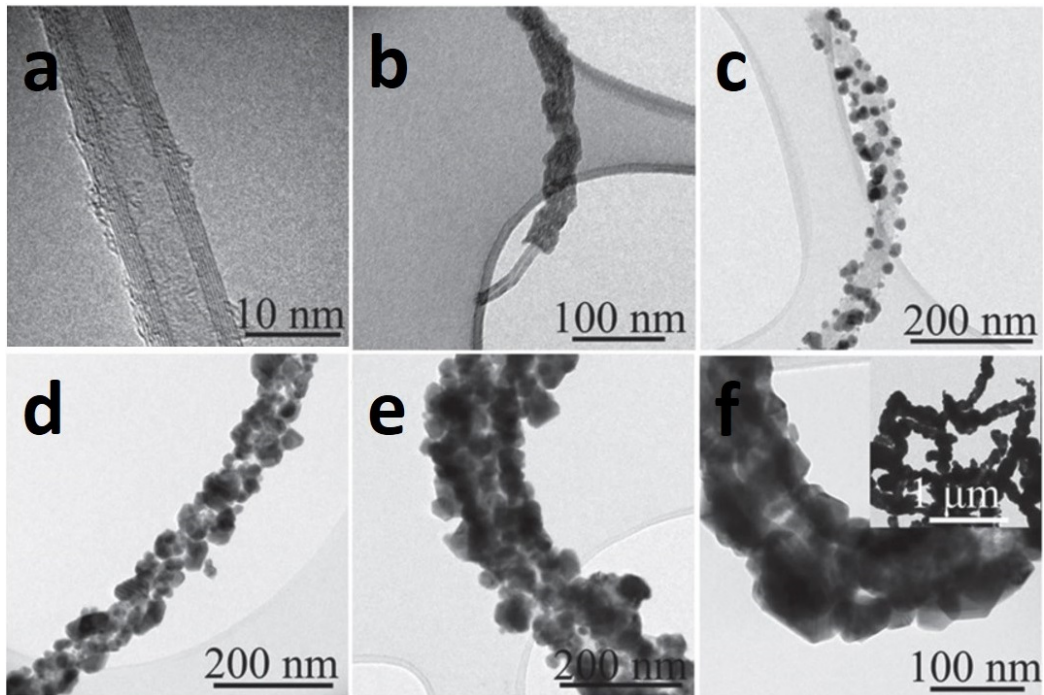


Figure 3.22: (a) A pure CNT with a diameter of 10 nm. (b) Silica-around-CNT shell structure. An amorphous silica layer with a thickness about 10 nm was deposited at the surface of APTES-CNTs. (c-f) Functionalized CNT-based hybrid nanowires prepared with different silver nitrate concentrations: (c) 1 g/L; (d) 5 g/L ; (e) 10 g/L; (f) 15 g/L, the inset shows the zoom-out image of the nanowire network. (from Paper E)

4

APPLICATIONS

In this chapter, the process technologies described in chapter 3 are combined and integrated for the fabrication of novel interconnect structures based on both aligned and randomly dispersed CNTs. The use of CNT-based interconnects in conventional applications, such as bumps and through silicon vias (TSVs), are demonstrated. Flexible, stretchable and transparent interconnect applications are also demonstrated. For the bumps and TSVs, the research focuses more on the process compatibility with the existing and established manufacturing flows, while for non-conventional flexible, stretchable, and transparent interconnects, the research focuses more on the exploration of unique CNT properties to satisfy the demand of these applications.

Sections 4.1, 4.2, 4.3, 4.4 and 4.5 correspond to the attached papers C, D, E, F and G. To be concise, these sections only summarize the highlights of the published papers. Each section starts with a brief background discussion, and proceeds with the major achievement highlighted. One or two abstract figures are taken from the corresponding papers to provide a better perception of the demonstrators. For the complete documentation of each application demonstrator, please refer to the attached full texts of the papers and their online supplements.

4.1 BUMP INTERCONNECTS

Bump interconnect is a very common part of an electronic system. Bumps are usually used to connect the silicon die to the external circuits, such as the printed circuit boards and the silicon interposers [80]. As the size of the electronic systems keeps shrinking, it is demanded to increase the bump density and to reduce the bump footprint. The trend to scale down the bump interconnect has brought up various challenges for the traditional metal materials. Thermally and mechanically related failures are further exacerbated by the increases in interconnect density, number of layers, and power consumption [81].

In order to cope with these challenges, Paper C proposed a novel process to use the CNTs as the bump interconnect. To start with, the pattern of the bumps was prepared by standard photolithography on a silicon wafer. Alumina and iron were evaporated onto the wafer sequentially using an e-beam evaporator. The wafer was cut into small chips and put into the CNT growth chamber for the synthesis

4.2 THROUGH SILICON VIAS

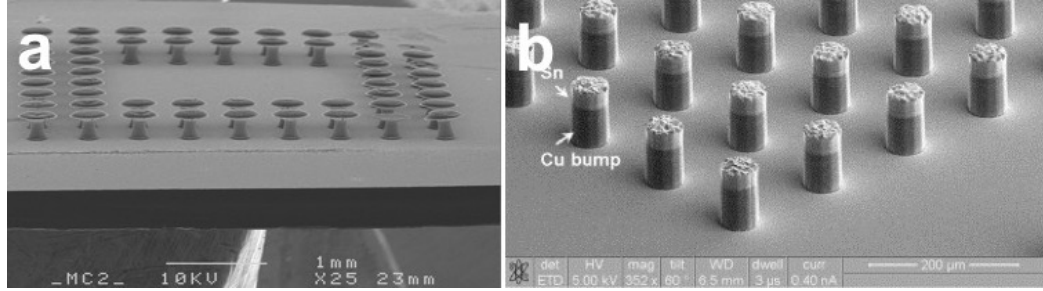


Figure 4.1: SEM micrograph of (a) transferred CNT bumps and (b) traditional copper-tin based bumps (reference [82]).

of CNTs by thermal CVD method. The grown CNTs were densified and sputter-coated with titanium and gold metal thin films. Finally the CNTs were transferred onto the indium-coated target substrate. Figure 4.1a, b show the picture of a resulting CNT bump array, in comparison with a traditional metal bump array. Most CNTs were transferred with their densified structures intact.

The resistance of the transferred CNT bundles was measured by the standard four-probe method. The extrapolated resistance of one bundle is around 3.7Ω . The I-V curve exhibits good linearity during the voltage sweep, which confirms the good contact between the CNTs and the indium-coated substrate. The estimated resistivity of such a bump can be derived given the rough dimensions of the bump (Figure 4.1a), with the simplification that the bundle is a $160\text{-}\mu\text{m}$ -wide and $350\text{-}\mu\text{m}$ -high cylinder. The corresponding resistivity is calculated to be around $2.1 \times 10^{-4} \Omega\cdot\text{m}$. This resistivity value is still much higher than those of the typical metals, i.e. copper or aluminum, mainly due to low quality CVD-grown CNTs. However, in turn, the CNTs suffer much less from electromigration-introduced degradation and thermal coefficient mismatch, which makes it a possible rival in applications where reliability plays the most critical role.

4.2 THROUGH SILICON VIAS

Stacking of circuits in the third dimension is one of the key technologies for future silicon scaling, and through silicon vias (TSVs) play a critical role in realizing this vision. However, TSVs made of metals usually have issues such voiding, extrusion, electromigration, and various thermal-mechanically induced reliability problems [83–85].

In Paper D, an improved method for fabricating CNT-based TSV interconnects is demonstrated and characterized, which complies with the temperature requirement of the existing device fabrication flow. CVD growth, paper/vapor densification, sputter coating and polymer transfer processes described in chapter 3 were used in the fabrication of the CNT TSVs.

One of the main features of this work is the hollow hexagonal CNT design introduced in an effort to obtain high aspect ratio CNT vias. Using this hexagonal

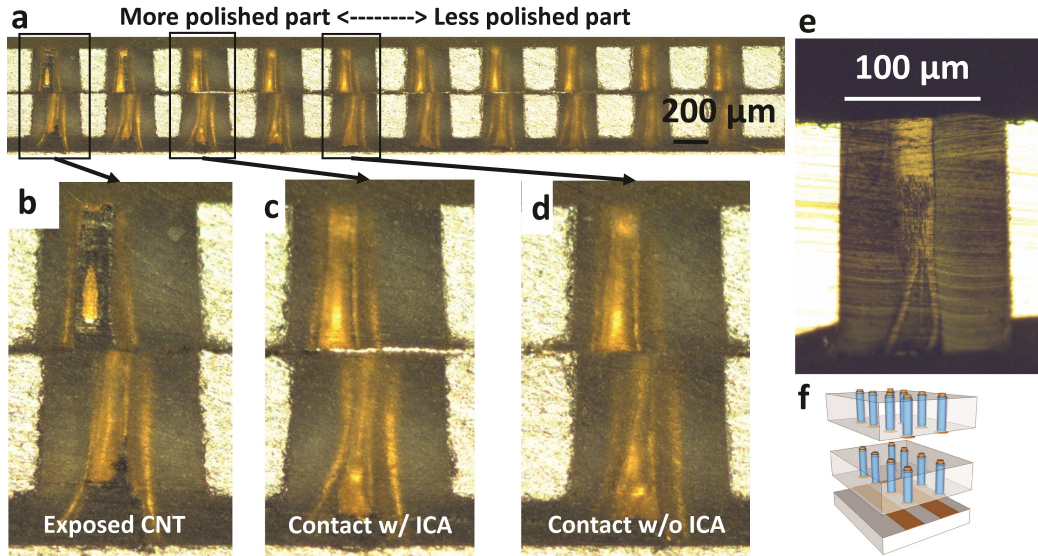


Figure 4.2: (a) Optical image of ten stacked CNT vias pairs in a row. (b) Two stacked CNT vias with exposed black CNT cores. (c,d) Two stacked CNT vias with and without ICA. Densified hexagonal structures can be seen through the semi-transparent polished polymer. (e) The cross-section of a densified CNT via with 30 μm in diameter and 30 μm in height. (f) Illustration of the double layer CNT TSV stacking scheme. (from Paper D)

design, aspect ratios of 10:1 were obtained. This is a considerable improvement over commonly adapted cylindrical bundles, which tends to get distorted for aspect ratios larger than 4:1 [86].

To stack the TSVs, the wafers were cut, aligned, stacked and bonded using the epoxy resin as a non-conductive bonding material (Figure 4.2f). One stacked sample was polished for cross-section examination as shown in Figure 4.2a. Unfortunately, the cross-sectioning was not 100% aligned to the CNT array. On the other hand, this fact made it possible to observe different aspects of the CNT vias along the cross-section. For the left-side vias, the cross-sectioning reached the core of the CNT bundles, thus exposing the black CNTs (Figure 4.2b). For the right-side vias, the cross-sectioning stopped just before the CNT core, thereby leaving the densified hexagonal structure fully visible through the semi-transparent polymer filling (Figure 4.2c,d). To further illustrate the possibility of scaling down this process, the cross-section of a high aspect ratio densified CNT-filled via with 30 μm in diameter is shown in Figure 4.2e.

The resistances of a number of different CNT via structures were measured during the development of this process using the four-probe method. The vias were around 400 μm in height and 100 μm in diameter. The resistances of hexagonal CNT structures covered with a titanium/gold metal layer decrease with the increasing gold layer thickness. Increasing the gold layer thickness from 50 nm to 200 nm decreases the resistance by a factor of four (from about 4 Ω to about

4.3 FLEXIBLE AND STRETCHABLE INTERCONNECTS

1 Ω). This would give a resistivity ranging from $7.6 \times 10^{-5} \Omega \cdot \text{m}$ to $1.6 \times 10^{-5} \Omega \cdot \text{m}$, if the CNT bundles were approximated to be cylindrical. The resistance of the hexagonal via structure ($0.85 \pm 0.05 \Omega$) was also compared to the resistance of the solid cylindrical via structure ($0.69 \pm 0.06 \Omega$), and little difference was observed. Additionally, the resistance of a two-layer stacked hexagonal via is $1.5 \pm 0.1 \Omega$. These results show that the metal coating on the CNTs did have positive effect on resistivity, thus it is possible to use improved metallic plating or doping methods to further improve the overall conductance of the system [87, 88].

4.3 FLEXIBLE AND STRETCHABLE INTERCONNECTS

Flexible interconnects are another interesting application for CNT-based materials. Contrary to the normally stiff and fatigue-prone metals, CNTs are mechanically robust and flexible, which made them a good candidate for flexible interconnects. Paper E presents a new flexible functionalized CNT-based hybrid nanowires and its application in the field of flexible and stretchable conductors.

Silver-coated randomly dispersed CNT networks were fabricated using the solution coating technology described in section 3.4.2. These CNT hybrid nanowires were deposited onto the silicon substrate through the patterning of a shadow silicon mask and embedded inside the PDMS substrate to form conductive wires. Figure 4.3a shows the parallel patterns of a 20-wire array with each wire having a length of 15 mm and a width of 500 μm . The inset in Figure 4.3a shows the wires at the bending state. It can be seen that the conductive lines remained both continuous and uniform when rolled up to 180° , with no indication of breakage or voids. Figure 4.3b shows another example of conductors with different patterns.

The degree of silver nanoparticle coverage on CNT surfaces plays a crucial factor in the electrical performance of the conductors. It has been found that the sheet resistance of the conductor decreases rapidly with increasing silver nitrate concentrations during the chemical coating, compared to the reference sample made from pure CNTs (1316 Ω/sq , resistivity of $1.3 \times 10^4 \Omega \cdot \mu\text{m}$). For samples prepared with silver nitrate concentrations of 1, 2, 5, and 10 g/L, the sheet resistance values are 100, 4, 0.38, and 0.15 Ω/sq , respectively, and the percolation threshold for an exponential decrease in resistance was located at 2 g/L (Figure 4.3d). It indicates that silver nanoparticles at the CNT surface were interconnecting and provide the main contribution to electrical conductivity when the silver nitrate concentration reached 2 g/L. The minimum sheet resistance (0.096 Ω/sq , resistivity of 0.96 $\Omega \cdot \mu\text{m}$) was reached when the CNTs were fully covered with silver nanoparticles ($C_{\text{AgNO}_3} = 15 \text{ g/L}$). These results are consistent with the morphology change of the functionalized CNT-based hybrid nanowires as observed by TEM in section 3.4.2, Figure 3.22c-f.

The bending effect on the sheet resistance of the CNT-based hybrid nanowires was investigated further on a high precision load/displacement measurement ma-

4.3 FLEXIBLE AND STRETCHABLE INTERCONNECTS

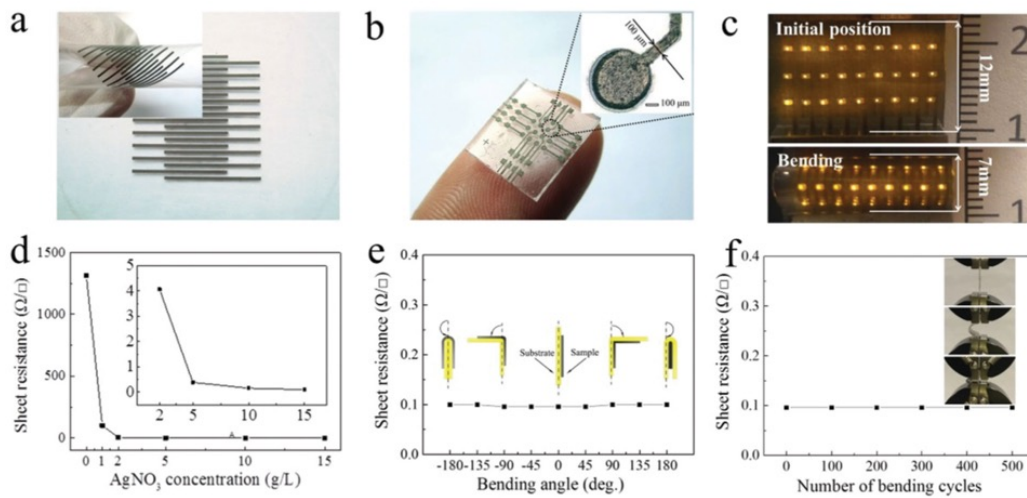


Figure 4.3: (a) Conductor patterns with 10+10 lines, each line has a length of 15 mm and a width of 500 μm . The inset shows the optical images of bending (180°). (b) Optical image of a conductor chip (8 mm \times 8 mm) with a minimum pad diameter of 100 μm . (c) Optical images of the LED array integrated by the flexible conductors with and without bending. The LEDs remained lit with the same illumination intensity when the demonstrator was bent to 180°. (d) Electrical tests show a decrease of sheet resistance with the increase of silver nanoparticles coverage on the CNTs. A minimum sheet resistance of 0.096 Ω/sq (equivalent resistivity of 0.96 $\Omega\cdot\mu\text{m}$) at 0% strain was obtained when CNT was totally covered by silver. (e) The sheet resistance change of the flexible conductors (concentration of $\text{AgNO}_3 = 15 \text{ g/L}$) as a function of bending angle. (f) Resistance results of the conductor after cycled bending. The conductor demonstrated a high reliability after 500 cycles of bending. (from Paper E)

4.4 FLEXIBLE AND TRANSPARENT INTERCONNECTS

chine¹. Figure 4.3e shows the sheet resistance variation of the flexible conductors as a function of bending angles (-180° to 180°). After an additional 500-cycle bending test, the conductor resistance remained constant, as shown in Figure 4.3f. These results show the excellent electro-mechanical stability of the hybrid nanowires during the bending tests. To further demonstrate the electrical stability of the conductors during bending, an array of light emitting diodes (LED) was assembled on the top of the parallel wires and sealed with PDMS. Figure 4.3c shows the lit image of the LEDs before and during bending. The LED illumination intensity at the bending state remained almost unchanged, which indicates the stable electrical performance of the flexible conductors.

The electrical performance of the nanowires was also investigated as a function of tensile strain on the same load/displacement machine. After the first cycle of stretching/releasing under 30% strain, the electrical resistance was restored to a stable value, with a resistance increase of around 30%. After a following 500-cycle of repeated stretching, the conductors showed relatively stable sheet resistance (0.35 Ω /sq at the strain of 0%) with a small variation of less than 8%, with no observed indication of failure. These results demonstrate the good electro-mechanical reliability and stability of these CNT-based conductors when compared with other reported CNT and silver nanowire composites [89–91].

4.4 FLEXIBLE AND TRANSPARENT INTERCONNECTS

Flexibility and transparency can be equally important for applications such as artificial skins [92], electronic eye cameras [93] and functional fabrics [94]. Researchers have been using various approaches to find a balance between transparency, resistivity, mechanical stability, manufacturability and many other application-specific properties. Shape-engineered metals, carbon nanotubes and graphene are among the mostly studied materials for these applications [3]. Conventional metal materials (e.g. titanium, gold, etc.) made into wavy shapes have good conductivity, and the processing methods for the deposition and etching of these materials are well established [95]. However, metals usually suffer from problems such as fatigue [4], degradation in air [96] and poor adhesion to most common flexible substrates [97, 98]. Recently, flexible and transparent conductors based on metal nanowires have been widely studied and they offer the best performance in terms of sheet resistance and manufacturability [99–101]. However, the resistance and transparency of the nanowire systems is dependent on the nanowire size and the network density. On the other hand, novel CNT- and graphene-based materials usually have better bending and stretching performance owing to their unique nano-structures. Yet their fabrication methods usually involve complicated and non-standard dispersion, doping and patterning techniques [3], which hinders the industrial adoption of these materials. In addition, CNT- and graphene-based materials usually have higher electrical resistance compared with that of the metals. Metal nanowires and

¹ Microtester, Instron

CNTs also have difficulties in making fine feature lines due to their large-aspect-ratio nature.

Paper F presents a fin-like metal/CNT (Fin-M/CNT) hybrid structure devised for the flexible and transparent conductor applications. Lithographically-patterned high aspect ratio CNT forests are synthesized by chemical vapor deposition. These forests are used as the supporting scaffold for a multi-layer metal film. Liquid form PDMS was used to infiltrate the metal/CNT hybrid structure, serving as a flexible substrate after being cured.

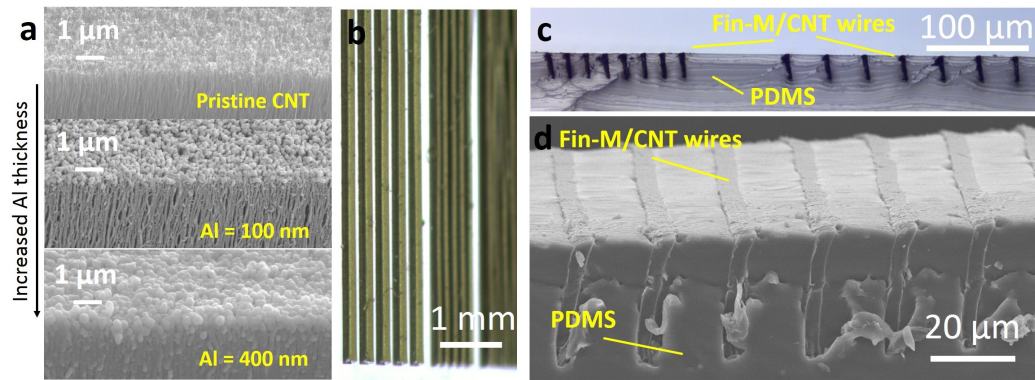


Figure 4.4: (a) SEM micrograph showing the morphology changes of the CNT bundle surface after metal sputtering. The thickness of the aluminum coating increased from 0 to 400 nm. (b) Stereo optical micrograph of the Fin-M/CNT wires with varying width of up to 180 μm (c) Optical micrograph of the cross section of the Fin-M/CNT wires with 5 μm width and 10 μm /20 μm pitches. (d) Micrograph of the cross section of the Fin-M/CNT wires. The sample was cut open with a knife. (from Paper F)

A set of Fin-M/CNT wires of different widths from 20 to 180 μm were fabricated to demonstrate the scalability of our proposed methods (Figure 4.4b). The SEM micrographs in Figure 4.4a show the formation of the continuous metal film on the surface of the pristine CNT scaffold with different metal thickness. Figure 4.4c shows an optical micrograph of the cross-sectional area of the 5 μm wide Fin-M/CNT wires embedded in PDMS for two different wire pitches (10 μm and 20 μm). Further SEM examination of these fine features is shown in Figure 4.4d. It can be concluded that the fine-featured Fin-M/CNT wires were completely infiltrated by PDMS with no voiding inside the porous CVD CNT forests.

In addition to the straight-line wire patterns, a honeycomb-like grid pattern was designed and fabricated using the proposed Fin-M/CNT structures (Figure 4.5a). The grid wire pitch is 1 mm and all samples have an aluminum coating with a thickness of 400 nm (Figure 4.5b). Due to the large PDMS-filled areas in between the grid lines, the resulting sample is a transparent conductive sheet (Figure 4.5c). The optical transmittances in the visible light range (390 nm to 700 nm) for samples with wire widths of 15 μm , 30 μm , 45 μm and 60 μm were plotted in Figure 4.5d along with their respective sheet resistance. Also shown in the same figure are the

4.4 FLEXIBLE AND TRANSPARENT INTERCONNECTS

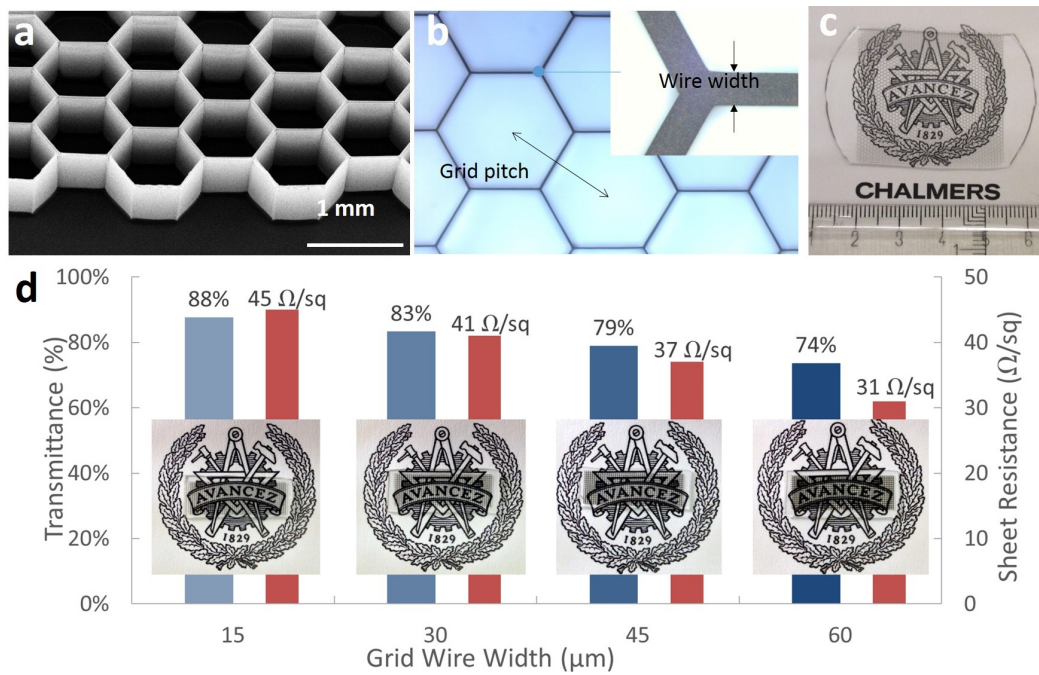


Figure 4.5: (a) SEM micrograph of the honeycomb-like grid pattern of the Fin-M/CNT structure after being transferred onto the thermal tape. (b) Top view optical micrograph of the grid Fin-M/CNT wires embedded in PDMS substrate and the zoom-in picture at the grid line junction. (c) A 34 mm × 34 mm rectangular transparent Fin-M/CNT conductor sheet with ruler and underlying logo. (d) Sheet resistance and transparency change with respect to grid wire width of 15 μm , 30 μm , 45 μm and 60 μm . The left vertical axis of the figure is for optical transmittance of the conductor in visible light range (390-700 nm) and the right vertical axis is for the corresponding sheet resistance values. (from Paper F)

optical pictures of the transparent samples placed on top of the Chalmers Avancez logotype. It is shown that for a wire width of 15 μm , a sheet resistance as low as 45 Ω/sq was obtained with an optical transmittance of 88%. This result shows a lower sheet resistance than those previously reported transparent sheet conductors based on thin layers of carbon nanotubes (65-80 Ω/sq , reference [102, 103]) and graphene (210-350 Ω/sq , reference [104–106]) at similar optical transmittance levels. For wire width of 60 μm , the sheet resistance was reduced to 31 Ω/sq , at the cost of the optical transmittance being reduced to 74%. The logotype insets in Figure 4.5d also show that the right-most sample was visually darker than the left-most sample, as the transmittance gradually increased from 74% to 88%. The largest transparent grid-patterned Fin-M/CNT sheet produced in this work is around 34 mm \times 34 mm (Figure 4.5c), a limitation set by the size of the CNT growth chamber.

The effect of bending on the sheet resistance of the Fin-M/CNT-based transparent conductor was investigated. The corresponding initial sheet resistance of the three samples were 85 Ω , 65 Ω and 45 Ω . After 500 cycles of bending at an angle of 180°, the electrical resistance of all samples remained almost constant (less than $\pm 5\%$ change during and after the tests). Good bonding between the Fin-W/CNT wire and PDMS substrate was retained after the bending test. Here a comparison can be made with a study on a graphene based conductor, that showed a resistance increase of 20% after the third bending cycle due to the crack formation [107]. The improved bonding with the substrate and excellent flexibility of the CNT scaffolds make the Fin-M/CNT wires less vulnerable to bending-related fatigue.

4.5 3D INTERCONNECTS FOR FLEXIBLE CIRCUIT INTEGRATION

A lot of research has been done in stacking electronic integrated circuits in the vertical direction for rigid electronic systems. On the contrary, there has been little research on the 3D integration scheme for making flexible electronics systems. Most polyimide and polyester based flexible electronics systems are fabricated in a similar manner as the rigid printed circuit boards [108]. There are also many polymer and silicone based approaches of fabricating flexible active and passive circuit components using novel materials such as CNTs and graphene [104, 109–115]. These approaches provide possibilities to make new types of flexible electronics other than the conventional ones. Yet most of these approaches are laying the functional circuits in a 2D plane.

Paper G demonstrates a flexible and stackable 3D interconnect system based on metal-coated CNT scaffolds embedded in PDMS substrate. The interconnect scaffold consists of patterned CNT forests of two different heights, which are obtained in a one-step CVD process by using two different underlayer materials (Al_2O_3 and SiO_2) underneath the iron catalyst. A low 100 μm thick CNT forest forms the core of the horizontal interconnect, while a 400 μm high CNT bundle defines the top-to-bottom via wiring. To complete the interconnect, the CNT scaffold was sputter-coated by a titanium/gold multi-metal layer and embedded in PDMS. The

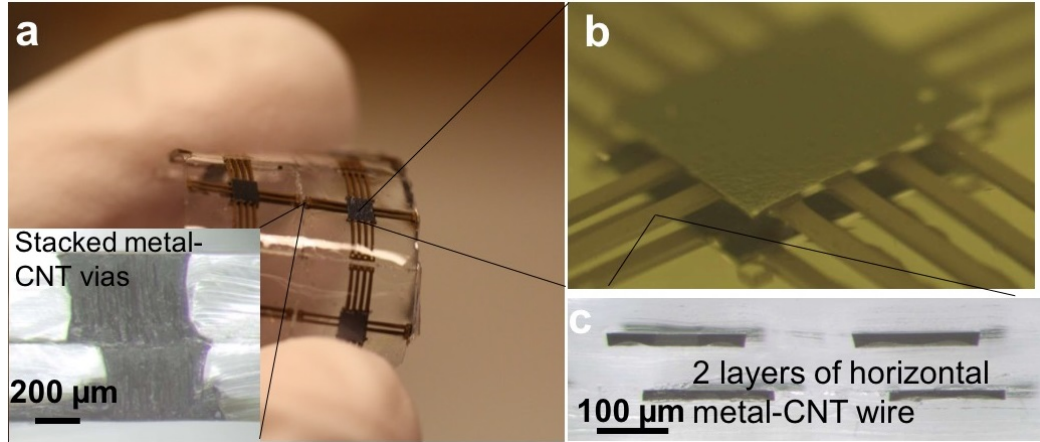


Figure 4.6: A two-layer 3D metal-CNT interconnect system with dummy silicon chips embedded in PDMS substrate. (a) The system in the bended status. Inset is the cross section picture of stacked vertical vias through the PDMS. Image obtained by cutting the PDMS open with a knife. (b) Zoom-in picture of the two-layer stacked chips in the flexible PDMS substrate. (c) The cross section of the two-layer horizontal wires embedded and running inside in the PDMS. (from Paper G)

substrate thickness were chosen to provide the possibility of embedding thinned silicon chips to form a stacked 3D flexible circuit system.

Dummy silicon chips thinned down to 100 μm were placed on the horizontal wires before PDMS filling, in order to demonstrate the possibility of stacking multiple chips in the vertical dimension (Figure 4.6a, b). The cross-section micrographs of the stacked horizontal and vertical interconnects are shown in Figure 4.6a, c.

Four-probe DC resistance of a single layer 3D metal-CNT interconnect system was measured with vias of 400 μm in height and 600 μm in diameter, and wires of 4 mm in length, 400 μm in width and 100 μm in thickness. For wires with titanium thickness fixed at 20 nm and gold thickness varied at 50 nm, 100 nm and 200 nm, their respective resistances were around 265 Ω, 89 Ω and 30 Ω. Compared to the resistance of pristine CNTs at 4796 Ω, the electrical performance was clearly improved by the metal coatings. The effect of bending on the sheet resistance of the 3D metal-CNT structures was also investigated. Experiment showed that there was no significant resistance increase after the bending test of 300 cycles.

To further investigate the mechanical properties of the structures, a finite element model with similar structural dimensions to the samples was developed (Figure 4.7). The mechanical properties of the PDMS and the CNTs for simulation were taken from Paper C and references [116, 117], respectively. A time-resolved bending simulation was applied to this model, which mimics the bending setup of the load/displacement machine. Figure 4.7a animates the bending motion of the PDMS structure and Figure 4.7b animates the bending of the CNTs embedded inside. It is shown that most of the strain deformation was absorbed by the PDMS material (Figure 4.7c, maximum 17-19%). The CNT structure only takes

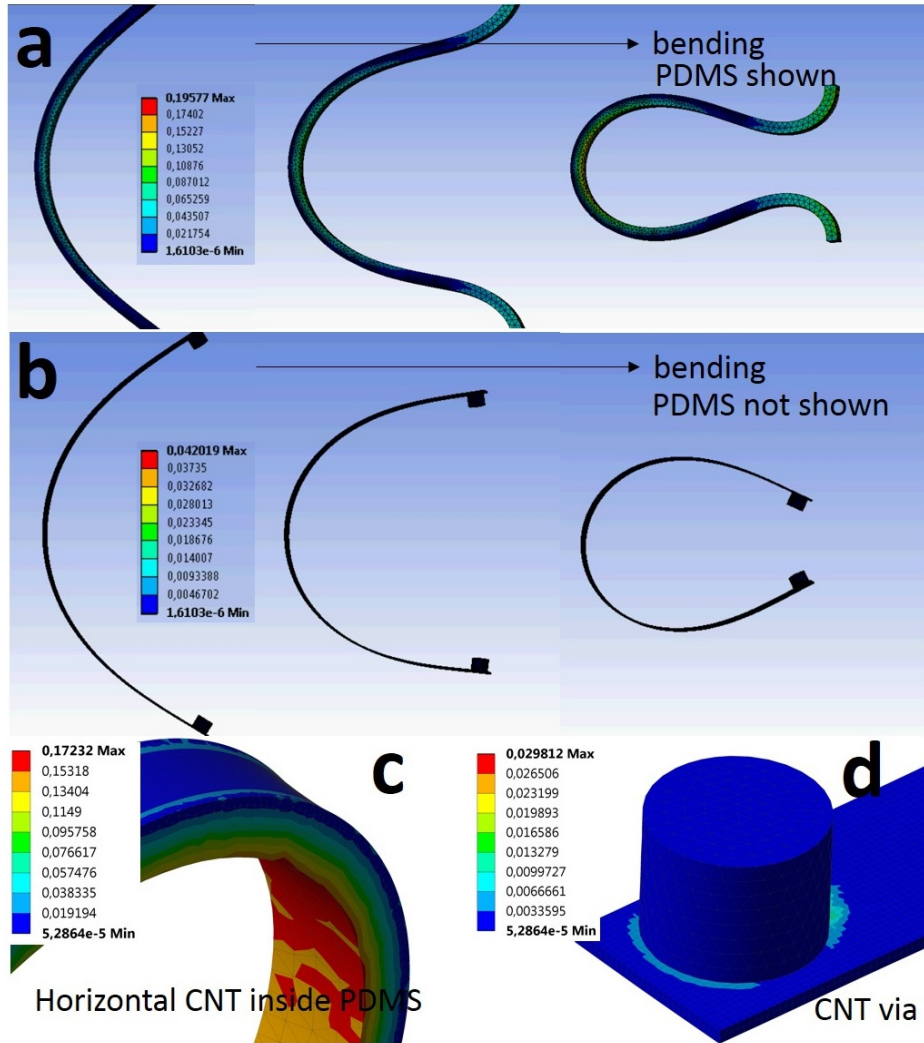


Figure 4.7: Finite element model of the CNT structures embedded in PDMS substrate. (a) The PDMS structures at different bending status during the time-resolved simulation. (b) The CNT horizontal wire and vertical via structures at different bending status during the same simulation. (c) The strain distribution in the PDMS substrate as in the most bended status of (a). The maximum strain deformation of the PDMS material is around 17-19%. (d) The strain deformation of the CNT wire and via structures as in the most bended status of (b). Only a fraction of the maximum strain (around 3-4%) was observed on the CNT structures. (from Paper G)

4.5 3D INTERCONNECTS FOR FLEXIBLE CIRCUIT INTEGRATION

a fraction of the strain (Figure 4.7d, maximum 3-4%). The model indicates that the softer, viscoelastic PDMS around of the metal-CNT structures absorbs much of the strain and the via area is almost strain-free during the bending test. This simulation complies with the experiment result that the resistance of the samples was stable after the bending tests.

CONCLUSION

By the writing of this thesis and the attached publications, this doctoral study explored the possibility of using carbon nanotubes (CNTs) as the interconnect material for electronics applications. The unique properties of CNTs are discussed for their potential as an alternative to metal-based interconnects. Different CNT process methods, such as growth, densification, transfer and coating, have been developed and discussed in detail within the scope of this thesis. Effort has been spent to find the ways of manipulating and improving the high temperature grown, defective and porous CNT bundles. These methods, together with other device fabrication techniques, are combined to demonstrate the feasibility of using CNTs in various electronic interconnect applications. Rigid and flexible interconnect scenarios are both covered with respective technology demonstrators, including bumps, through silicon vias (TSVs), and flexible/stretchable/transparent conductors.

For the rigid CNT interconnects, high yield bumps have been fabricated and characterized for mechanical and electrical performance. A novel process flow, based on densifying and transferring vertically aligned CNT structures, has been devised to fabricate highly uniform CNT bump arrays at chip scale.

TSVs consisting of densified CNT bundles in the via core have been also demonstrated. Double-layer stacked chips with CNT TSVs have been successfully fabricated and characterized. CNTs with a minimum via diameter of 30 μm and an aspect ratio of 10:1 have been demonstrated with specially designed hexagonal geometries. This process is compatible with the temperature requirement of the existing device fabrication process, and the test results indicate good stability and scalability.

For the flexible CNT interconnects, a novel silver plating method has been developed for stretchable conductor applications. Flexible and stretchable circuits based on silver-coated CNT networks showed stable electro-mechanical performance in both bending and stretching tests.

Furthermore, low resistance fin-like metal/CNT hybrid interconnect structures have been devised. High aspect ratio CNT/metal structures were embedded in a flexible substrate with the help of PDMS infiltration. Hexagonal grid patterns were designed for transparent conductive sheets with high optical transparency, low sheet resistance and excellent robustness against bending.

CONCLUSION

Stacking of the flexible interconnect systems has been achieved using the catalyst-engineered CNT forest growth. Different CNT growth underlayers were designed to produce height-differentiated CNT structures, which act as the scaffolds for the metallic conducting paths in a three dimensional manner. Stacking of the interconnects into 3D networks, with dummy chips embedded in each layer, has been demonstrated.

The process technology developed in this thesis is just a small amount of the technological development required to see the adoption of CNT-based interconnects in industry. There is still a long way ahead before the commercialization of CNTs in mass-produced electronic devices.

Nevertheless, I wish that the process work presented in this thesis will provide some valuable guidance for future researchers whose work may involve new materials of similar properties.

ACKNOWLEDGMENT

I want to express my gratitude to all the people who helped me during this doctoral study.

I would like to thank Prof. Johan Liu for the opportunity to work in this fascinating field. Special thanks should be attributed to Dr. Teng Wang and Dr. Yifeng Fu who provided profound advices and knowledge in the cleanroom and CNT process technologies. And my deepest gratitude goes to Prof. Kjell Jeppson who has always been the most valuable mentor whenever I need guidance.

I am grateful for all the staff of the Nanofabrication Lab in MC2. They have made the lab a wonderful place to work. I also want to express my thanks to all my colleagues in the EMSL lab (formerly BNSL). It is a great honor to work with you.

Last but not least, I would like to thank my family for their unconditional love and encouragement throughout my research.

BIBLIOGRAPHY

- [1] Zsolt Tokei, Kristof Croes, Gerald P. Beyer. Reliability of copper low-k interconnects. *Microelectronic Engineering*, 87(3):348 – 354, 2010.
- [2] Cheng-Ta Ko, Kuan-Neng Chen. Reliability of key technologies in 3d integration. *Microelectronics Reliability*, 53(1):7–16, 2013.
- [3] John a Rogers, Takao Someya, Yonggang Huang. Materials and mechanics for stretchable electronics. *Science*, 327(5973):1603–1607, 2010.
- [4] X J Sun, C C Wang, J Zhang, G Liu, G J Zhang, X D Ding, G P Zhang, J Sun. Thickness dependent fatigue life at microcrack nucleation for metal thin films on flexible substrates. *Journal of Physics D: Applied Physics*, 41(19):195404, 2008.
- [5] Sumio Iijima. Helical microtubules of graphitic carbon. *Nature*, 354(6348):56–58, 1991.
- [6] S. Frank, P. Poncharal, Z. L. Wang, W. A. De Heer. Carbon nanotube quantum resistors. *Science*, 280(5370):1744–1746, 1998.
- [7] B. Q. Wei, R. Vajtai, P. M. Ajayan. Reliability and current carrying capacity of carbon nanotubes. *Applied Physics Letters*, 79(8):1172–1174, 2001.
- [8] David Mann, Ali Javey, Jing Kong, Qian Wang, Hongjie Dai. Ballistic transport in metallic nanotubes with reliable Pd ohmic contacts. *Nano Lett.*, 3(11):1541–1544, 2003.
- [9] Jun Li, Qi Ye, Alan Cassell, Hou Tee Ng, Ramsey Stevens, Jie Han, M. Meyyappan. Bottom-up approach for carbon nanotube interconnects. *Applied Physics Letters*, 82(15):2491–2493, 2003.
- [10] Hong Li, N. Srivastava, Jun-Fa Mao, Wen-Yan Yin, K. Banerjee. Carbon nanotube vias: Does ballistic electron-phonon transport imply improved performance and reliability? *Electron Devices, IEEE Transactions on*, 58(8):2689–2701, 2011.
- [11] F Kreupl, A.P Graham, G.S Duesberg, W Steinhögl, M Liebau, E Unger, W Hönlein. Carbon nanotubes in interconnect applications. *Microelectronic Engineering*, 64(1-4):399–408, 2002.
- [12] Tianhua Yu, E. Kim, N. Jain, Yang Xu, R. Geer, Bin Yu. Carbon-based interconnect: Performance, scaling and reliability of 3d stacked multilayer

BIBLIOGRAPHY

- graphene system. *Electron Devices Meeting (IEDM), IEEE International*. IEEE, 2011.
- [13] Geza Toth, Jani Mäklin, Niina Halonen, Jaakko Palosaari, Jari Juuti, Heli Jantunen, Krisztian Kordas, W. Gregory Sawyer, Robert Vajtai, Pulickel M. Ajayan. Carbon-Nanotube-Based electrical brush contacts. *Advanced Materials*, 21(20):2054–2058, 2009.
- [14] Daisuke Yokoyama, Takayuki Iwasaki, Tsuyoshi Yoshida, Hiroshi Kawarada, Shintaro Sato, Takashi Hyakushima, Mizuhisa Nihei, Yuji Awano. Low temperature grown carbon nanotube interconnects using inner shells by chemical mechanical polishing. *Applied Physics Letters*, 91(26):263101, 2007.
- [15] N. Srivastava, K. Banerjee. Performance analysis of carbon nanotube interconnects for vlsi applications. *Computer-Aided Design, IEEE/ACM International Conference on*, 2005.
- [16] R. R. Keller, M. C. Strus, A. N. Chiamonti, Y. L. Kim, Y. J. Jung, D. T. Read. Reliability testing of advanced interconnect materials. *AIP Conference Proceedings*, 1395(1):259–263, 2011.
- [17] Mizuhisa Nihei, Masahiro Horibe, Akio Kawabata, Yuji Awano. Simultaneous formation of multiwall carbon nanotubes and their end-bonded ohmic contacts to ti electrodes for future ULSI interconnects. *Japanese Journal of Applied Physics*, 43:1856–1859, 2004.
- [18] A.P. Graham, G.S. Duesberg, R. Seidel, M. Liebau, E. Unger, F. Kreupl, W. Hönlein. Towards the integration of carbon nanotubes in microelectronics. *Diamond and Related Materials*, 13(4–8):1296–1300, 2004.
- [19] Veena Choudhary, Anju Gupta. Polymer/Carbon nanotube nanocomposites. Siva Yellampalli, redaktor, *Carbon Nanotubes - Polymer Nanocomposites*. InTech, 2011.
- [20] Hyoung Joon Choi, Jisoon Ihm, Steven G. Louie, Marvin L. Cohen. Defects, quasibound states, and quantum conductance in metallic carbon nanotubes. *Physical Review Letters*, 84(13):2917–2920, 2000.
- [21] M. S. Dresselhaus, G. Dresselhaus, P. Avouris. *Carbon nanotubes: synthesis, structure, properties, and applications*. Springer, 2001.
- [22] R. Saito, M. S. Dresselhaus. *Physical properties of carbon nanotubes*. Imperial College Press, 1998.
- [23] A. Javey, J. Kong. *Carbon nanotube electronics*. Springer, 2009.
- [24] H. J. Li, W. G. Lu, J. J. Li, X. D. Bai, C. Z. Gu. Multichannel ballistic transport in multiwall carbon nanotubes. *Physical Review Letters*, 95(8):1–4, 2005.

- [25] P. M. Ajayan, T. W. Ebbesen, T. Ichihashi, S. Iijima, K. Tanigaki, H. Hiura. Opening carbon nanotubes with oxygen and implications for filling. *Nature*, 362(6420):522–525, 1993.
- [26] L. Zhu, Y. Xiu, D. W. Hess, C.-P. Wong. Aligned carbon nanotube stacks by water-assisted selective etching. *Nano Letters*, 5(12):2641–2645, 2005.
- [27] D. Yokoyama, T. Iwasaki, T. Yoshida, H. Kawarada, S. Sato, T. Hyakushima, M. Nihei, Y. Awano. Low temperature grown carbon nanotube interconnects using inner shells by chemical mechanical polishing. *Applied Physics Letters*, 91(26):263101, 2007.
- [28] P. Poncharal, C. Berger, Y. Yi, Z. L. Wang, W. A. de Heer. Room temperature ballistic conduction in carbon nanotubes. *The Journal of Physical Chemistry B*, 106(47):12104–12118, 2002.
- [29] C. T. White, T. N. Todorov. Carbon nanotubes as long ballistic conductors. *Nature*, 393(6682):240–242, 1998.
- [30] P. G. Collins, M. Hersam, M. Arnold, R. Martel, Ph. Avouris. Current saturation and electrical breakdown in multiwalled carbon nanotubes. *Physical Review Letters*, 86(14):3128, 2001.
- [31] T. Ragab, C. Basaran. Joule heating in single-walled carbon nanotubes. *Journal of Applied Physics*, 106(6):063705, 2009.
- [32] H. Dai, E. W. Wong, C. M. Lieber. Probing electrical transport in nanomaterials: conductivity of individual carbon nanotubes. *Science*, 272(5261):523–526, 1996.
- [33] J. Hone, M. Whitney, C. Piskoti, A. Zettl. Thermal conductivity of single-walled carbon nanotubes. *Physical Review B*, 59(4):R2514, 1999.
- [34] P. Kim, L. Shi, A. Majumdar, P. L. McEuen. Thermal transport measurements of individual multiwalled nanotubes. *Physical Review Letters*, 87(21):215502, 2001.
- [35] S. Berber, Y.-K. Kwon, D. Tománek. Unusually high thermal conductivity of carbon nanotubes. *Physical Review Letters*, 84(20):4613–4616, 2000.
- [36] J. Che, T. Cagin, W. A. Goddard III. Thermal conductivity of carbon nanotubes. *Nanotechnology*, 11(2):65–69, 2000.
- [37] N. Mingo, D. A. Broido. Carbon nanotube ballistic thermal conductance and its limits. *Physical Review Letters*, 95(9):096105, 2005.
- [38] O. Lourie, H. D. Wagner. Evaluation of young’s modulus of carbon nanotubes by micro-raman spectroscopy. *Journal of Materials Research*, 13(9):2418–2422, 1998.

BIBLIOGRAPHY

- [39] M.-F. Yu, O. Lourie, M. J. Dyer, K. Moloni, T. F. Kelly, R. S. Ruoff. Strength and breaking mechanism of multiwalled carbon nanotubes under tensile load. *Science*, 287(5453):637–640, 2000.
- [40] M.-F. Yu, B. S. Files, S. Arepalli, R. S. Ruoff. Tensile loading of ropes of single wall carbon nanotubes and their mechanical properties. *Physical Review Letters*, 84(24):5552, 2000.
- [41] G. Overney, W. Zhong, D. Tománek. Structural rigidity and low frequency vibrational modes of long carbon tubules. *Zeitschrift für Physik D Atoms, Molecules and Clusters*, 27(1):93–96, 1993.
- [42] J. P. Lu. Elastic properties of carbon nanotubes and nanoropes. *Physical Review Letters*, 79(7):1297, 1997.
- [43] G. Gao, T. Cagin, W. A. Goddard III. Energetics, structure, mechanical and vibrational properties of single-walled carbon nanotubes. *Nanotechnology*, 9(3):184–191, 1998.
- [44] D. A. Walters, L. M. Ericson, M. J. Casavant, J. Liu, D. T. Colbert, K. A. Smith, R. E. Smalley. Elastic strain of freely suspended single-wall carbon nanotube ropes. *Applied Physics Letters*, 74(25):3803–3805, 1999.
- [45] C. Li, T.-W. Chou. Elastic properties of single-walled carbon nanotubes in transverse directions. *Physical Review B*, 69(7):073401, 2004.
- [46] H. Jiang, B. Liu, Y. Huang, K. C. Hwang. Thermal expansion of single wall carbon nanotubes. *Journal of Engineering Materials and Technology*, 126(3):265–270, 2004.
- [47] M. R. Falvo, G. J. Clary, R. M. Taylor II, V. Chi, F. P. Brooks Jr., S. Washburn, R. Superfine. Bending and buckling of carbon nanotubes under large strain. *Nature*, 389(6651):582–584, 1997.
- [48] Ting Guo, Pavel Nikolaev, Andrew G. Rinzler, David Tomanek, Daniel T. Colbert, Richard E. Smalley. Self-assembly of tubular fullerenes. *The Journal of Physical Chemistry*, 99(27):10694–10697, 1995.
- [49] Yucheng Lan, Yang Wang, Z. F. Ren. Physics and applications of aligned carbon nanotubes. *Advances in Physics*, 60(4):553–678, 2011.
- [50] Mukul Kumar, Yoshinori Ando. Chemical vapor deposition of carbon nanotubes: A review on growth mechanism and mass production. *Journal of Nanoscience and Nanotechnology*, 10(6):3739–3758, 2010.
- [51] R S Wagner, W C Ellis. Vapor-liquid-solid mechanism of crystal growth and its application to silicon. *Transactions of the metallurgical society of AIME*, 233(6):1053, 1965.

- [52] Anne-Claire Dupuis. The catalyst in the CCVD of carbon nanotubes—a review. *Progress in Materials Science*, 50(8):929–961, 2005.
- [53] Guofang Zhong, Takayuki Iwasaki, Kotaro Honda, Yukio Furukawa, Iwao Ohdomari, Hiroshi Kawarada. Low temperature synthesis of extremely dense and vertically aligned single-walled carbon nanotubes. *Japanese Journal of Applied Physics*, 44(No. 4A):1558–1561, 2005.
- [54] S. Sato, M. Nihei, A. Mimura, A. Kawabata, D. Kondo, H. Shioya, T. Iwai, M. Mishima, M. Ohfuti, Y. Awano. Novel approach to fabricating carbon nanotube via interconnects using size-controlled catalyst nanoparticles. *International Interconnect Technology Conference (IITC)*, 2006.
- [55] Guangtong Liu, Yuanchun Zhao, Ke Deng, Zheng Liu, Weiguo Chu, Jingran Chen, Yanlian Yang, Kaihong Zheng, Haibo Huang, Wenjun Ma, Li Song, Haifang Yang, Changzhi Gu, Guanghui Rao, Chen Wang, Sishen Xie, Lianfeng Sun. Highly dense and perfectly aligned single-walled carbon nanotubes fabricated by diamond wire drawing dies. *Nano Letters*, 8(4):1071–1075, 2008.
- [56] B. L. Wardle, D. S. Saito, E. J. Garcia, A. J. Hart, R. G. de Villoria, E. A. Verploegen. Fabrication and characterization of ultrahigh-volume-fraction aligned carbon nanotube-polymer composites. *Advanced Materials*, 20(14):2707–2714, 2008.
- [57] Nirupama Chakrapani, Bingqing Wei, Alvaro Carrillo, Pulickel M. Ajayan, Ravi S. Kane. Capillarity-driven assembly of two-dimensional cellular carbon nanotube foams. *Proceedings of the National Academy of Sciences of the United States of America*, 101(12):4009–4012, 2004.
- [58] Huan Liu, Shuhong Li, Jin Zhai, Huanjun Li, Quanshui Zheng, Lei Jiang, Daoben Zhu. Self-Assembly of Large-Scale micropatterns on aligned carbon nanotube films. *Angewandte Chemie International Edition*, 43(9):1146–1149, 2004.
- [59] Michael De Volder, Sameh H. Tawfick, Sei Jin Park, Davor Copic, Zhouzhou Zhao, Wei Lu, A. John Hart. Diverse 3D microarchitectures made by capillary forming of carbon nanotubes. *Advanced Materials*, 22(39):4384–4389, 2010.
- [60] Teng Wang, Kjell Jeppson, Johan Liu. Dry densification of carbon nanotube bundles. *Carbon*, 48(13):3795–3801, 2010.
- [61] D. N. Futaba, K. Miyake, K. Murata, Y. Hayamizu, T. Yamada, S. Sasaki, M. Yumura, K. Hata. Dual porosity single-walled carbon nanotube material. *Nano Letters*, 9(9):3302–3307, 2009.

BIBLIOGRAPHY

- [62] A. Cao, P.L. Dickrell, W.G. Sawyer, M.N. Ghasemi-Nejhad, P.M. Ajayan. Super-compressible foamlike carbon nanotube films. *Science*, 310(5752):1307, 2005.
- [63] SuhrJ., VictorP., CiL., SreekalaS., ZhangX., NalamasuO., AjayanP. M. Fatigue resistance of aligned carbon nanotube arrays under cyclic compression. *Nat Nano*, 2(7):417–421, 2007.
- [64] Shaoming Huang, Liming Dai, Albert W. H. Mau. Patterned growth and contact transfer of well-aligned carbon nanotube films. *J. Phys. Chem. B*, 103(21):4223–4227, 1999.
- [65] I. Soga, D. Kondo, Y. Yamaguchi, T. Iwai, M. Mizukoshi, Y. Awano, K. Yube, T. Fujii. Carbon nanotube bumps for LSI interconnect. *Electronic Components and Technology Conference ECTC*. IEEE, 2008.
- [66] Ashavani Kumar, Victor L. Pushparaj, Swastik Kar, Omkaram Nalamasu, Pulickel M. Ajayan, Rajashree Baskaran. Contact transfer of aligned carbon nanotube arrays onto conducting substrates. *Applied Physics Letters*, 89(16):163120, 2006.
- [67] Teng Wang, Björn Carlberg, Martin Jonsson, Goo-Hwan Jeong, Eleanor E. B. Campbell, Johan Liu. Low temperature transfer and formation of carbon nanotube arrays by imprinted conductive adhesive. *Applied Physics Letters*, 91(9):093123, 2007.
- [68] Yifeng Fu, Yiheng Qin, Teng Wang, Si Chen, Johan Liu. Ultrafast transfer of Metal-Enhanced carbon nanotubes at low temperature for Large-Scale electronics assembly. *Advanced Materials*, 22(44):5039–5042, 2010.
- [69] Ashavani Kumar, Victor L. Pushparaj, Swastik Kar, Omkaram Nalamasu, Pulickel M. Ajayan, Rajashree Baskaran. Contact transfer of aligned carbon nanotube arrays onto conducting substrates. *Applied Physics Letters*, 89(16):163120, 2006.
- [70] Lingbo Zhu, Kyoung-Sik Moon, B. Bertram, D.W. Hess, C.P. Wong. Assembling carbon nanotube bundles using transfer process for fine-pitch electrical interconnect applications. *Electronic Components and Technology Conference ECTC*, 2007.
- [71] M.T. Barako, Yuan Gao, A.M. Marconnet, Mehdi Asheghi, Kenneth E. Goodson. Solder-bonded carbon nanotube thermal interface materials. *13th IEEE Intersociety Conference on Thermal and Thermomechanical Phenomena in Electronic Systems (ITherm)*, 2012.
- [72] Teng Wang, Kjell Jeppson, Niklas Olofsson, Eleanor E B Campbell, Johan Liu. Through silicon vias filled with planarized carbon nanotube bundles. *Nanotechnology*, 20(48):485203, 2009.

- [73] Yifeng Fu, Teng Wang, Johan Liu, Xiaojing Wang, Yan Zhang. Carbon nanotubes as cooling fins in microelectronic systems. *9th IEEE Conference on Nanotechnology (IEEE-NANO)*, 2009.
- [74] Teng Wang, Björn Carlberg, Martin Jönsson, Goo-Hwan Jeong, Eleanor E. B. Campbell, Johan Liu. Low temperature transfer and formation of carbon nanotube arrays by imprinted conductive adhesive. *Applied Physics Letters*, 91(9):093123, 2007.
- [75] Hongjin Jiang, Lingbo Zhu, Kyoung-Sik Moon, Yi Li, C.P. Wong. Low temperature carbon nanotube film transfer via conductive adhesives. *57th Electronic Components and Technology Conference (ECTC)*, 2007.
- [76] Teng Wang, Kejll Jeppson, Lilei Ye, Johan Liu. Carbon-nanotube through-silicon via interconnects for three-dimensional integration. *Small*, 7(16):2313–2317, 2011.
- [77] Johannes Svensson, Eleanor E. B. Campbell. Schottky barriers in carbon nanotube-metal contacts. *Journal of Applied Physics*, 110(11), 2011.
- [78] Y Zhang, Nathan W Franklin, Robert J Chen, Hongjie Dai. Metal coating on suspended carbon nanotubes and its implication to metal-tube interaction. *Chemical Physics Letters*, 331(1):35–41, 2000.
- [79] Seong Chu Lim, Jin Ho Jang, Dong Jae Bae, Gang Hee Han, Sunwoo Lee, In-Seok Yeo, Young Hee Lee. Contact resistance between metal and carbon nanotube interconnects: Effect of work function and wettability. *Applied Physics Letters*, 95(26), 2009.
- [80] R. R. Tummala. *Fundamentals of microsystems packaging*. McGraw-Hill, 2001.
- [81] Report on interconnects, international technology roadmap for semiconductors (ITRS). 2011.
- [82] Kung-Liang Lin, Edward-Yi Chang, Lin-Chi Shih. Evaluation of cu-bumps with lead-free solders for flip-chip package applications. *Microelectronic Engineering*, 86(12):2392–2395, 2009.
- [83] S.-K. Ryu, K.-H. Lu, T. Jiang, J.-H. Im, R. Huang, P. S. Ho. Effect of thermal stresses on carrier mobility and keep-out zone around through-silicon vias for 3-d integration. *Device and Materials Reliability, IEEE Transactions on*, 12(2):255 –262, 2012.
- [84] L. W. Kong, J. R. Lloyd, M. Liehr, A. C. Rudack, S. Arkalgud, A. C. Diebold. Measuring thermally induced void growth in conformally filled through-silicon vias (TSVs) by laboratory x-ray microscopy. *Proceedings of SPIE*, 8324(1):832412, 2012.

BIBLIOGRAPHY

- [85] C. Cassidy, J. Kraft, S. Carniello, F. Roger, H. Ceric, A. P. Singulani, E. Langer, F. Schrank. Through silicon via reliability. *Device and Materials Reliability, IEEE Transactions on*, 12(2):285–295, 2012.
- [86] Michael De Volder, Sameh H. Tawfick, Sei Jin Park, Davor Copic, Zhouzhou Zhao, Wei Lu, A. John Hart. Diverse 3D microarchitectures made by capillary forming of carbon nanotubes. *Advanced Materials*, 22(39):4384–4389, 2010.
- [87] Yao Zhao, Jinqun Wei, Robert Vajtai, Pulickel M. Ajayan, Enrique V. Barrera. Iodine doped carbon nanotube cables exceeding specific electrical conductivity of metals. *Scientific Reports*, 1, 2011.
- [88] Chandramouli Subramaniam, Takeo Yamada, Kazufumi Kobashi, Atsuko Sekiguchi, Don N. Futaba, Motoo Yumura, Kenji Hata. One hundred fold increase in current carrying capacity in a carbon nanotube-copper composite. *Nature Communications*, 4, 2013.
- [89] Taehoon Kim, Hyunsoo Song, Jaeheung Ha, Sangwoo Kim, Donghyun Kim, Seungjun Chung, Jaemyon Lee, Yongtaek Hong. Inkjet-printed stretchable single-walled carbon nanotube electrodes with excellent mechanical properties. *Applied Physics Letters*, 104(11):–, 2014.
- [90] Tsuyoshi Sekitani, Yoshiaki Noguchi, Kenji Hata, Takanori Fukushima, Takuzo Aida, Takao Someya. A rubberlike stretchable active matrix using elastic conductors. *Science*, 321(5895):1468–1472, 2008.
- [91] Sungryul Yun, Xiaofan Niu, Zhibin Yu, Weili Hu, Paul Brochu, Qibing Pei. Compliant silver nanowire-polymer composite electrodes for bistable large strain actuation. *Advanced Materials*, 24(10):1321–1327, 2012.
- [92] Kuniharu Takei, Toshitake Takahashi, Johnny C Ho, Hyunhyub Ko, Andrew G Gillies, Paul W Leu, Ronald S Fearing, Ali Javey. Nanowire active-matrix circuitry for low-voltage macroscale artificial skin. *Nature materials*, 9(10):821–826, 2010.
- [93] Heung Cho Ko, Mark P Stoykovich, Jizhou Song, Viktor Malyarchuk, Won Mook Choi, Chang-Jae Yu, Joseph B Geddes, Jianliang Xiao, Shuodao Wang, Yonggang Huang, John a Rogers. A hemispherical electronic eye camera based on compressible silicon optoelectronics. *Nature*, 454(7205):748–753, 2008.
- [94] Massimo Barbaro, Alessandra Caboni, Piero Cosseddu, Giorgio Mattana, Annalisa Bonfiglio. Active devices based on organic semiconductors for wearable applications. *IEEE Transactions on Information Technology in Biomedicine*, 14(3):758–766, 2010.

- [95] R Verplancke, F Bossuyt, D Cuypers, J Vanfleteren. Thin-film stretchable electronics technology based on meandering interconnections: fabrication and mechanical performance. *Journal of Micromechanics and Microengineering*, 22(1):015002, 2011.
- [96] Po-Chun Hsu, Hui Wu, Thomas J Carney, Matthew T McDowell, Yuan Yang, Erik C Garnett, Michael Li, Liangbing Hu, Yi Cui. Passivation coating on electrospun copper nanofibers for stable transparent electrodes. *ACS nano*, 6(6):5150–5156, 2012.
- [97] Sukanta De, Thomas M Higgins, Philip E Lyons, Evelyn M Doherty, Peter N Nirmalraj, Werner J Blau, John J Boland, Jonathan N Coleman. Silver Nanowire Networks as Flexible, Transparent, Conducting Films: Extremely High DC to Optical Conductivity Ratios. *ACS nano*, 3(7):1767–1774, 2009.
- [98] Frederik S. F. Morgenstern, Dinesh Kabra, Sylvain Massip, Thomas J. K. Brenner, Philip E. Lyons, Jonathan N. Coleman, Richard H. Friend. Ag-nanowire films coated with ZnO nanoparticles as a transparent electrode for solar cells. *Applied Physics Letters*, 99(18):183307, 2011.
- [99] Sukjoon Hong, Junyeob Yeo, Jinhwan Lee, Habeom Lee, Phillip Lee, Seung S. Lee, Seung Hwan Ko. Selective Laser Direct Patterning of Silver Nanowire Percolation Network Transparent Conductor for Capacitive Touch Panel. *Journal of Nanoscience and Nanotechnology*, 15(3):2317–2323, 2015.
- [100] Phillip Lee, Jooyeun Ham, Jinhwan Lee, Sukjoon Hong, Seungyong Han, Young Duk Suh, Sang Eon Lee, Junyeob Yeo, Seung Seob Lee, Dongjin Lee, Seung Hwan Ko. Highly Stretchable or Transparent Conductor Fabrication by a Hierarchical Multiscale Hybrid Nanocomposite. *Advanced Functional Materials*, 24(36):5671–5678, 2014.
- [101] Seungyong Han, Sukjoon Hong, Jooyeun Ham, Junyeob Yeo, Jinhwan Lee, Bongchul Kang, Phillip Lee, Jinhyeong Kwon, Seung S Lee, Min-Yang Yang, Seung Hwan Ko. Fast plasmonic laser nanowelding for a Cu-nanowire percolation network for flexible transparent conductors and stretchable electronics. *Advanced Materials*, 26(33):5808–14, 2014.
- [102] David S Hecht, Amy M Heintz, Roland Lee, Liangbing Hu, Bryon Moore, Chad Cucksey, Steven Risser. High conductivity transparent carbon nanotube films deposited from superacid. *Nanotechnology*, 22(7):075201, 2011.
- [103] Jong Hyuk Yim, Yong Seok Kim, Ken Ha Koh, Soonil Lee. Fabrication of transparent single wall carbon nanotube films with low sheet resistance. *Journal of Vacuum Science & Technology B: Microelectronics and Nanometer Structures*, 26(2):851, 2008.
- [104] Keun Soo Kim, Yue Zhao, Houk Jang, Sang Yoon Lee, Jong Min Kim, Kwang S Kim, Jong-Hyun Ahn, Philip Kim, Jae-Young Choi, Byung Hee

BIBLIOGRAPHY

- Hong. Large-scale pattern growth of graphene films for stretchable transparent electrodes. *Nature*, 457(7230):706–710, 2009.
- [105] Xuesong Li, Yanwu Zhu, Weiwei Cai, Mark Borysiak, Boyang Han, David Chen, Richard D Piner, Luigi Colombo, Rodney S Ruoff. Transfer of large-area graphene films for high-performance transparent conductive electrodes. *Nano letters*, 9(12):4359–4363, 2009.
- [106] Yu Wang, Xiaohong Chen, Yulin Zhong, Furong Zhu, Kian Ping Loh. Large area, continuous, few-layered graphene as anodes in organic photovoltaic devices. *Applied Physics Letters*, 95(6):063302, 2009.
- [107] Zongping Chen, Wencai Ren, Libo Gao, Bilu Liu, Songfeng Pei, Hui-Ming Cheng. Three-dimensional flexible and conductive interconnected graphene networks grown by chemical vapour deposition. *Nature materials*, 10(6):424–428, 2011.
- [108] B. Chou, S. Beilin, H. Jiang, D. Kudzuma, M. Lee, M. McCormack, T. Massingill, M. Peters, J. Roman, Y. Takahashi, V. Wang. Multilayer high density flex technology. *49th Electronic Components and Technology Conference*. IEEE, 1999.
- [109] Dong Ming Sun, Chang Liu, Wen Cai Ren, Hui Ming Cheng. A review of carbon nanotube- and graphene-based flexible thin-film transistors. *Small*, 9(8):1188–1205, 2013.
- [110] Takeo Yamada, Yuhei Hayamizu, Yuki Yamamoto, Yoshiki Yomogida, Ali Izadi-Najafabadi, Don N Futaba, Kenji Hata. A stretchable carbon nanotube strain sensor for human-motion detection. *Nature Nanotechnology*, 6(5):296–301, 2011.
- [111] Shinya Aikawa, Erik Einarsson, Theerapol Thurakitserree, Shohei Chiashi, Eiichi Nishikawa, Shigeo Maruyama. Deformable transparent all-carbon-nanotube transistors. *Applied Physics Letters*, 100(6):63502, 2012.
- [112] Chen Feng, Kai Liu, Yeah Sheng Wu, Liang Liu, Jia Shyong Cheng, Yuying Zhang, Yinghui Sun, Qunqing Li, Shoushan Fan, Kaili Jiang. Flexible, stretchable, transparent conducting films made from superaligned carbon nanotubes. *Advanced Functional Materials*, 20(6):885–891, 2010.
- [113] Yingying Zhang, Chris J. Sheehan, Junyi Zhai, Guifu Zou, Hongmei Luo, Jie Xiong, Y. T. Zhu, Q. X. Jia. Polymer-embedded carbon nanotube ribbons for stretchable conductors. *Advanced Materials*, 22(28):3027–3031, 2010.
- [114] Le Cai, Li Song, Pingshan Luan, Qiang Zhang, Nan Zhang, Qingqing Gao, Duan Zhao, Xiao Zhang, Min Tu, Feng Yang, Wenbin Zhou, Qingxia Fan, Jun Luo, Weiya Zhou, Pulickel M Ajayan, Sishen Xie. Super-stretchable,

- transparent carbon nanotube-based capacitive strain sensors for human motion detection. *Scientific reports*, 3:3048, 2013.
- [115] Chih Fan Hu, Wang Shen Su, Weileun Fang. The integration of cnts-based flexible tactile sensor and flexible circuit by polymer molding process. *16th International Solid-State Sensors, Actuators and Microsystems Conference*, 2011.
- [116] Yin Ji Ma, Xue Feng Yao, Quan Shui Zheng, Ya Jun Yin, Dong Jie Jiang, Guang Hui Xu, Fei Wei, Qiang Zhang. Carbon nanotube films change poisson's ratios from negative to positive. *Applied Physics Letters*, 97(6), 2010.
- [117] Tae Kyung Kim, Jeong Koo Kim, Ok Chan Jeong. Measurement of nonlinear mechanical properties of pdms elastomer. *Microelectronic Engineering*, 88(8):1982–1985, 2011.

Paper A

Formation of Three-dimensional Carbon Nanotube Structures by Controllable Vapor Densification

Teng Wang, Di Jiang, Si Chen, Kjell Jeppson, Lilei Ye, Johan Liu

Materials Letters, Volume 78, Pages 184-187, 2012

Paper B

Through-Silicon Vias Filled With Densified and Transferred Carbon Nanotube Forests

Teng Wang, Si Chen, Di Jiang, Yifeng Fu, Kjell Jeppson, Lilei Ye, Johan Liu
IEEE Electron Device Letters, Volume 33, Issue 3, Pages 420-422, 2012

